MSc Theses

Summaries of the student work conducted in the spring 2021

PRODUCTION AND MATERIALS ENGINEERING | DEPARTMENT OF MECHANICAL ENGINEERING SCIENCES
FACULTY OF ENGINEERING | LUND UNIVERSITY

Preface

The last two years has been an experience beyond our wildest belief. During this time our students at Production and Materials engineering have conducted their studies and have now finished their degree works. In this book we have gathered the summaries of the work handed in by our students. This has been a voluntary opportunity and 23 students has decided to contribute.

You will here have the opportunity to read about project conducting experiments on material characteristics, producibility tests and model development within our three branches of subject, production technology, material engineering and manufacturing systems.

Enjoy!

The full length of reports can be found onthe university home page at: https://lup.lub.lu.se/student-papers/search

Master Program Directors
Jinming Zhou and Christina Windmark






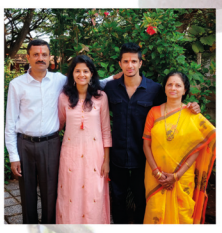



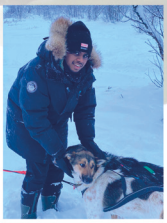

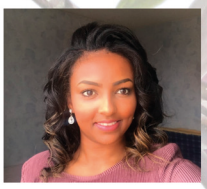


LUND UNIVERSITY

Photo: Petra Francke

MSc Program
Production and Materials Engineering

Mechanical Engineering Science

2021

Table of Contents

A comparative study of hole quality criteria in CFRP drilling

Jerome Paul Raenius Jeevanandham, Sakthivel Balaji

Department of Mechanical Engineering Sciences
Faculty of Engineering, Lund University
Lund, Sweden

ABSTRACT

Drilling is an essential hole-making operation in the modern industrial world. Drilling operation is comparatively challenging in composites when compared to metals. Composites are heterogeneous and possess a high strength-to-weight ratio which makes it a challenge in composite drilling. The hole quality has two major defects affecting the reliability of CFRP composites: Uncut fibers and delamination are critical factors responsible for gap formation, leading to loosening and slacking of the joints. This phenomenon has a high degree of risk in the reliability of joints. The drilling process of CFRP can be optimized using optimum tool geometry and cutting data.

This thesis analyzes hole quality factors such as the delamination and uncut fibers, aiming to find an optimum tool geometry for minimal tool wear. This thesis also aims to identify the key parameters which influence the formation of undesirable defects found in drilling composites. These hole quality defects influence negatively in bolted and riveted connection between CFRP components which is a significant safety concern in the Aerospace and Motorsports field.

During the initial phase, extensive research has been carried to gather data through literature surveys. This research was responsible for understanding the tool geometry influencing the defects such as Delamination or uncut fibers, which has set a foundation for the experimentation. The second phase entails analyzing CFRP specimens using Alicona Infinite Focus. Whereas, in the final stage, the data from the microscopic images are processed using MATLAB scripts to calculate and compare the delamination factor and uncut fibers under varying cutting conditions and tools.

The results are plotted using graphs to compare delamination and uncut fiber under varying cutting and tool coatings. The reason for the hole quality behavior has been discussed briefly in the later chapter.

Keywords: *CFRP drilling, Composites, Hole quality, Delamination, Uncut fibers*

1. INTRODUCTION

Drilling is an essential hole-making operation in the manufacturing field. In the case of composites, high strength ratio (4.5 GPa above), abrasive properties lead to intensive tool degradation and make it challenging to achieve tolerance in the hole-making process. However, tolerance is a crucial factor in manufacturing and assembling a product. Formation of hole defects such as **delamination** and **uncut fibers** were considered critical factors influencing the tolerance levels of the machined CFRP components. CFRP has been widely used in Aerospace, Motorsports, and sports equipment. The formation of delamination and uncut fibers in CFRP components leads to a gap in a joint bolt or rivet connection. This gap leads to loosening and slacking of the joints in CFRP components, which negatively impacts the reliability of these components. Especially in the aerospace industry, reliability is a crucial factor because of safety concerns. It is essential to achieve the desired tolerance and hole quality to meet the high standards. Various parameters such as tool geometry, tool type, and cutting data are responsible for the hole quality and tolerance. It is necessary to study and analyze the machining parameters to avoid hole quality defects. Improvements can be made through adopting suitable tool selection and cutting data for machining.

2. METHODOLOGY

The study of hole quality defect formation begins with an exploratory research in a literature survey. It also includes an explanatory research about the cause and effect of hole quality in CFRP defects such as uncut fibers and delamination. During the first phase, the quantitative data have been gathered to understand the science behind defect formation and composite drilling. Literature review has been performed on CFRP drilling, hole quality defects, uncut fibers and delamination. This is required to set up a foundation for our experimental work which is planned to be performed in the later stages of the thesis. During the second phase, the experiments are carried to study the hole quality defects via microscopic measurements using Alicona Infinite Focus. The Microscopic images are interpreted into data to calculate the delamination factor and uncut fibers using MATLAB special scripts. These values are been used to plot the graph to compare the delamination and uncut fibers under varying cutting conditions and tool coatings.

2.1. WORKPIECE MATERIAL

A series of CFRP drilling tests were part of the current investigation's experimental phase. Drilling was performed with an EMCO PC MILL 300 with a maximum rotation speed of 10000 rpm. A KISTLER 9129AA dynamometer with a KISTLER 5070 amplifier and a National Instrument 9223 ADC has

been used to measure axial force and torque during drilling. Drilling CFRP samples from the Saab AB company were used for the experimental phase of the current investigation (Sweden). It was a new type of PAN-type CFRP composite material that was used in the construction of modern Saab aircraft. A microscopy using an Alicona Infinite Focus 3D optical microscope was used to achieve structural analysis of a polished CFRP sample. CFRP samples were 4 mm thick and reinforced with a [45/90/-45/0]5s scheme. Each fiber ply is 200 mm thick. 70 percent of the CFRP was made up of fibers with a diameter of 7 µm. Plates measuring 70x70 mm were used to hold the samples. A unique workpiece holder was 3D printed and used. Without a substrate, it was possible to drill 26 holes in each plate.

2.2. Tools used

Cemented carbide and PCD drills were used for CFRP drilling with various cutting data. For comparison checking, the custom made PCD drill and uncoated cemented carbide SECO SD203A-8.0-27-8R drill bit have been used. Grinding was done on the rake and flank surfaces to provide identical geometry (in the tollerance range of 1-2 degrees). after grinding, Alicona Infinite Focus 3D optical microscope was used to measure the and confirm the drill geometry.

2.3. Analysis Algorithm

The proposed methodology is based on analysis of images of the drilled holes. The methodology is mainly based on six modules that are used in a sequential order. They are: (i) defining the circumference of the hole, (ii) defining the contours of the uncut fibers, (iii) defining the delaminated area, (iv) creating and analyzing the profiles of uncut fibers, (v) creating and analyzing the profiles of delamination, and (vi) estimating a general evaluation of hole quality.

The expected diameter, an image of the drilled hole, the scale of the image, and the measurement error are the input data. The expected diameter is normally the nominal diameter of the drill bit. This parameter is used for defining the actual hole circumference and for reducing the program runtime. Image resolution is a main factor for the accuracy of quality analysis. As the diameter of the fibers in most CFRP materials range from 7 to 15 µm, the density of pixels in the image should be high for a better analysis.

3. Hole quality

In composite, hole quality is major challenge in composites to thrive for because of their heterogenous nature and high strength to weight ratio. Hole quality parameters include entry delamination, hole size accuracy, circularity, and surface quality. There are various ways to optimize the drilling operation in composites to achieve tolerance and high hole quality such as tool geometry, cutting data and type of cutting tool used. Process parameters can be altered such as reducing the feed, thrust, and increasing the rotational speeds have shown significant hole quality changes in research experiments.

Delamination affects the strength of the carbon composites. Cutting tool interactions with CFRP could be complex because of its inhomogeneous and anisotropic structure. Delamination, fiber pull-out, burr, and matrix thermal degradation are being the side effects that are caused during the machining of stacks. Out of these all effects, pull-out delamination is considered as the critical one, it affects the load-carrying capacity and fatigue life drastically in a negative way. The large thrust force produced by the large point angle drills is usually responsible for the elastic deformation occurrence. Thrust force is the component of cutting force along the drill bit axis. Delamination has a very huge impact on reduction strength and the fatigue life of the CFRP. Most commonly, delamination occurs due to the punch on CFRP by the chisel edge of the tool and further developed by cutting edges. Therefore, thrust force should be limited to avoid the delamination. Choosing proper drilling parameters to reduce thrust force is essential.

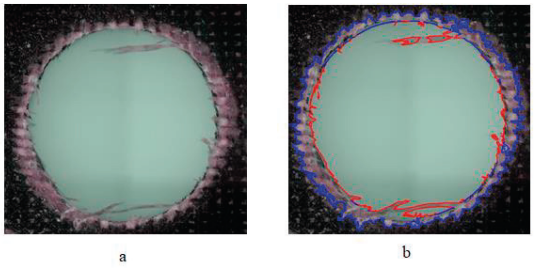

Figure 1: (a) drilled hole of a CFRP panel; (b) delaminated area of the drilled hole.

Figure 1: (a), shows the drilled hole and the defects caused in the hole, in the drilling process. Delamination commonly take place at the exit of the hole. The captured image is focused on the exit of the hole and the delamination zone is concentrated at the circumference of the hole, as illustrated. Chisel edge is a major reason for hole quality, especially delamination. Delamination occurs when the thrust force acting upon the chisel edge overcomes the interlaminar bond strength at the exit of the hole. On the other hand, drilling temperature could also induce delamination. Proper drilling parameters can be used to reduce thrust force. So, it is crucial to maintain critical temperature and thrust force to prevent delamination. To overcome delamination, it is effective to reduce feed rate gradually as hole exit approaches. The parameter that most affects the thrust force is the feed rate (by 90%). Although, the spindle speed is responsible only for 5 to 8% of

variation of the thrust force when the machining parameters change.

Uncut fibers and fiber pull-out mainly occur on the machined edges of CFRP composites when inappropriate cutting data is used. Uncut fibers usually do not negatively impact the mechanical properties of machined CFRP parts, but they necessitate additional machining operations, which increases the production time and efficiency in case their elimination is unavoidable. Uncut fibers can be removed by a deburring method. Burrs are generated mainly due to the fiber orientation angle of CFRP, the machining conditions, the tool geometry, and the tool material. A defect like delamination occurs when the thrust force exceeds a critical bending moment of the fiber and polymer layers. In uncut fibers, the defect is associated with the relationship between the fiber orientation and the cutting angle. Furthermore, uncut fibers tend to increase when tool wear increases.

4. RESULTS

The experiment was performed with eight different cutting data and two different tool coatings. The test results are compared to observe the hole quality defects based on the cutting parameters and tool coating.

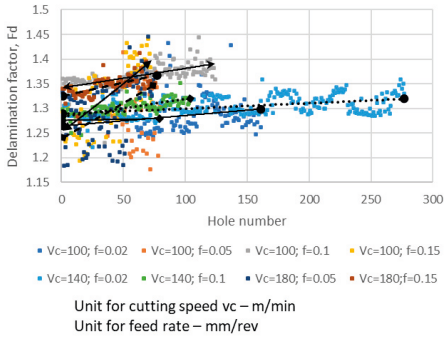

Figure 2: Comparison chart for delamination factor Fd

From the overall comparison of delamination factor, we could see that cutting conditions, cutting speed cutting speed vc 100 m/min, feed rate 0.15 mm/rev and cutting speed vc 140 m/min, feed rate 0.1mm/rev exhibits inclined trend. Whereas the rest of the cutting conditions have indicated slightly linear behavior. Cuttingcutting speed vc 100 m/min, feed rate 0.1 mm/rev and *vc* cutting speed vc 140 m/min, feed rate 0.02 mm/rev have the highest delamination factor range from 1.3 to 1.4. *vc* cutting speed vc 100 m/min, feed rate 0.02 mm02mm/rev and *vc*cutting speed vc 180 m/min, feed rate 0.05 mm/rev indicates lower range of delamination factors fromfactor i.e., 1.24 to 1.35.

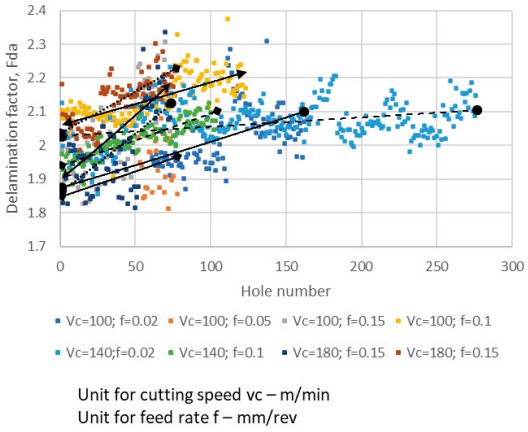

Figure 3: Comparison chart for adjusted delamination factor, Fda

From the overall comparison of adjusted delamination factor, we could see that cutting conditions, except *vc* cutting speed vc 140 m/min, feed rate 0.02 mm02mm/rev, have exhibited inclined trend. Whereas *vc* is cutting speed vc 140 m/min and feed of rate 0.02 mm02mm/rev have indicated slightly linear behavior. Speed ofcutting speed vc 180 m/min and feed of 0.15 mm/rev and *vc* m/min, feed rate 0.15mm/rev and cutting speed cutting speed vc 100 m/min, feed rate 0.1mm/rev have the highest delamination factor range from 2 to 2.25. Speed of cutting speed vc 100 m/min, feed rate 0.05 mm05mm/rev and *vc* cutting speed vc 100 m/min, feed rate 0.02 mm02mm/rev indicates lower range of delamination factor fromi.e., 1.85 to 2.

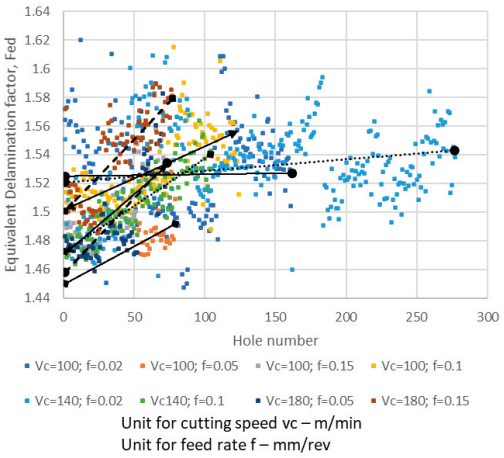

Figure 4: Comparison chart for Equivalent delamination factor Fed.

From the overall comparison of equivalent delamination factor, we could see that cutting conditions, except vccutting speed vc 140 m/min, feed rate 0.02 mm02mm/rev and vc cutting speed vc 100 m/min, feed rate 0.02 mm/rev, have exhibited inclined

trend. Whereas, vc cutting speed vc 140 m/min, feed rate 0.02 mm/rev and vc cutting speed vc 100 m/min, feed rate 0.02 mm02mm/rev, have indicated slightly linear behavior. Cutting speed vc 100 m/min, feed rate 0.1 mm1mm/rev and vc cutting speed vc 180 m/min, feed rate 0.15 mm15mm/rev have the highest delamination factor range from 1.5 to 1.58. Cuttingcutting speed ofvc 100 m/min, feed rate 0.05m/rev; vc05mm/rev; cutting speed vc 180 m/min, feed rate 0.05 mm05mm/rev and vccutting speed vc 100 m/min, f mm/rev, feed rate 0.15 mm15mm/rev indicates lower range of delamination factor i.e., 1.45 to 1.52.

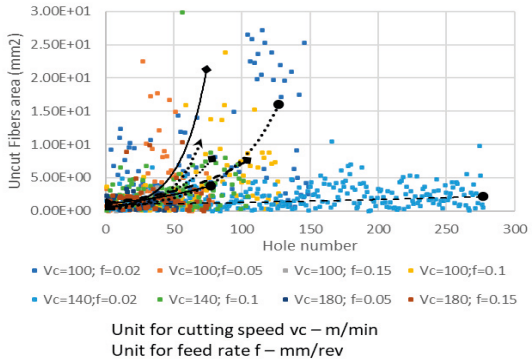

Figure 5: Comparison chart for uncut fiber area

From the figure, the comparison chart clearly shows the difference between each of the values and behavior of uncut fiber areas for different cutting data. Through overall comparison, we can identify that, the trendline behavior is almost identical for vc = cutting speed vc =180 m/min with feed rate f = 0.05 mm/rev and vc = cutting speed vc =100 m/min with feed rate f = 0.1 mm/rev, with a higher value of slope. The trendline for vc = cutting speed vc =140 m/min and feed rate f = 0.02 mm/rev, is almost linear, which shows the operation is steady throughout the panel and with good cutting conditions. As an overall comparison, it is identifiable that the uncut fiber values come under 10mm^2. Few spikes are also noted in the data, which may be caused due to the improper cutting conditions and overlapping caused during image processing.

5. DISCUSSION AND CONCLUSION

From the results obtained, we can conclude that for higher cutting speed and lower feed rate the range of the delamination area is much lower compared to lower cutting speed, as per figure. But, for lower cutting speed, the higher the feed rate the delamination area tends to be lower, up 15%. Even though change remains to be at 15% for all the varying parameters, it is significant when it comes to comparison point of view. The steady inclination in delamination area and uncut fiber area from 1st hole to the last hole, indicated that tool wear comes into action during the drilling process. The main reason for the delamination and uncut fiber being thrust force and tool wear, it is logical to conclude that during the process, with increase in number of holes drilled, the results obtained are as expected. The delamination factors Fd, Fda and Fed, are the variables that determine the actual hole quality. From the results obtained, the trendline shown in the Figure 4, indicated that the delamination factor also increases with increase in number of drilled holes, as maximum delamination diameter is directly proportional to delamination factor. Even though, the change is below 0.05, this comparative study clearly gives the necessary information about each cutting condition. A similar trend also takes into action for Fda and Fed, but with a higher magnitude because, both Fda and Fed takes both area of delamination and maximum delamination diameter into consideration, whereas Fd focuses only on maximum delamination diameter.

The irregularity in the diameter is one of the major reasons where Fed is the factor that is more accurate. Finally, as an overall conclusion it is evident to propose using the comparative study conducted, that for cutting speed *cutting speed vc* =100, 140 and 180 m/min, the results show promising quality of the holes. When compared to each other, the study shows that for higher cutting speed, the lower the feed rate, the delamination factor and uncut fibers tend to be lower. Whereas, for lower cutting speed, fluctuations are found within the range of delamination and uncut fibers, sliding slightly towards higher feed rate.

From the overall results obtained, and along with similar literature and theory, the results are quite adequate and compliments the outcome from this comparative study. So, it is not understated to conclude that the results obtained, and the comparison provided are reliable.

6. ACKNOWLEDGEMENTS

We are much obliged to thank the people who have guided and assisted us with valuable information throughout the work.

- Dr. Andrii Hrechuk, our Supervisor from the University.
- Dr. Christina Windmark, our course coordinator, Production of Materials Engineering.
- Professor Jan-Eric Ståhl, our Examiner.

Additionally, we would like to thank LTH for their support with resources.

7. REFERENCES

J. P. R. Jeevanandham and S. Balaji, "A comparative study on hole quality criteria in CFRP drilling," Lund University, Lund, 2021.

Axial cutting force in drilling operations

Bharath Gelli, Heaven Frezgi
Department of Mechanical Engineering Sciences
Faculty of Engineering, Lund University Lund, Sweden

ABSTRACT

Metal cutting has been part of industrial development since the iron age. Since then, it has changed shapes and criteria, but efficiency in metal cutting has been one of the biggest goals in the industrial world for just as long. To have maximum efficiency, it requires some level of process behavior prediction, which inspired the degree project. The project was conducted in collaboration with Lund University and Seco as an academic degree project for the university and as a practical tool for Seco.

The project started with a literature review, where existing models in the prediction of axial cutting force in drilling operations were thoroughly studied and analyzed. The result of the literature review was one chosen model for further tests and modifications. The chosen model was used to predict the axial cutting force for chosen tool diameters and feed machining SS2541 in the material group P5.

Experimental tests were performed to test the model. They showed that the prediction was not a perfect fit, which led to numerical tests where different solver-based constants were added to the model to provide the minimum possible error percentage between the measured and modeled axial cutting forces. During this phase of the project, a pattern was detected where the model underestimated the axial cutting force for smaller diameters.

The results are presented in performance order where the correlation between diameter, feed, measured, and modeled axial cutting force is both visualized in graphs and described in the report. Furthermore, a chapter with a suggestion for future studies has been added to optimize the model further.

Keywords: *Axial cutting force, Drilling, Model optimization.*

1. Introduction

The focus of this research is a prediction model for the axial cutting force in drilling operations. The model is of research interest due to its impact on the hole quality and process efficiency. The model created in this project will potentially be programmed in software applications to provide their customers an optimal operational condition. The model and the experiments only focus on the conventional drilling operation with 90 degrees of entrance angle. Parameters, such as hole quality and tool life, are not studied in this thesis.

The mathematical model should include the crucial parameters that affect the axial cutting forces and have as minimum error percentage as possible when compared to practical test results. Additionally, the model should be user-friendly, meaning that it should be easily used in Microsoft Excel, Mathcad, and other similar software. When investigating the existing models, the criteria described above will be in focus.

In general, a conventional solid drill consists of two cutting surfaces. During cutting, several chips are removed from the surface and pass through the flutes present on the drill bit. These flutes enable the chips to flow out easily. Most of the tools in the drilling operation consist of two cutting edges. The number of chip channels depends upon the number of main cutting edges. The chips after the machining process are simultaneously sent out through these chip channels. The quality of the drill is achieved when the right tool is used for the right material. Several tool parameters come into play while performing the drilling operation. See Figure 1.

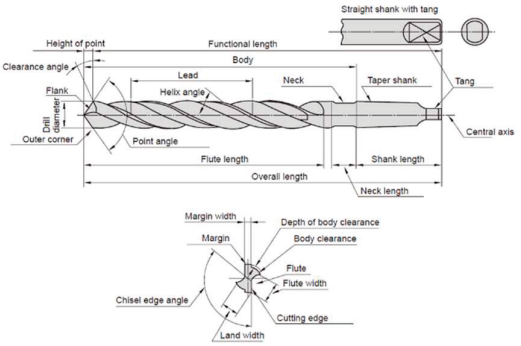

Figure 1: Visualization of tool geometry (Mitsubishi, Corporation Materials, 2019)

Steel and stainless steel are the workpiece materials that the project focuses on. Theoretically, steel includes all iron materials with carbon less than 2% carbon and 1% manganese and small amounts of silicon, phosphorus, sulfur, and oxygen. Meanwhile, stainless steel can be divided into four categories Martensitic, Ferritic, Austenitic, and Duplex steels.

2. Methodology

This project was conducted in three stages. The first stage was a thorough literature review of existing knowledge. Based on the outcome of the literature review and identified gaps, adequate and feasible experimental design and testing were planned and performed, which is the second stage. Cutting forces are collected using the Kistler Dynamometer for different tool geometry and cutting data and led to

the third stage gap analysis. A new model for predicting the axial cutting force in drilling operation was derived and reported based on the experimental work's outcome.

3. Chosen mathematical model.

The forces in the drilling operations are as follows:

- Axial force: The force acting along the axis of the drill.
- Radial force: The force acting along the radial direction.
- Tangential force: The force perpendicular to the other two force components (Axial and Radial).

Usually, the radial and tangential forces are represented as torque, but the axial force keeps as it is. This project is concentrated and limited only to the axial forces. The axial force affects flank wear rate, hole quality, and hole tolerances, which is why the axial force should be investigated and predicted as accurately as possible. The axial force is affected by feed rate and tool diameter.

In the practical handbook, part 2 of Sandvik Coromant (1994), the axial cutting force is calculated using the Equation below.

$$F_p = 0.5 * k_c * a_p * f_r * \sin k_r \quad (1)$$

Where: k_c - specific cutting force
a_p - radial depth of cut [mm]
f_r - axial feed rate [mm/rev]
k_r - entering angle
0.5 - constant in order to get the force per tooth

$$k_c = \frac{F_c}{A} = \frac{b * k_{c1.1} * h_{eW}^{1-mc}}{b * h_{eW}} = k_{c1.1} * h_{eW}^{-mc} \quad (1.1)$$

The specific cutting force (kc), also known as the tangential force, is required to machine a chip with a specific cross-section of one square millimeter. In equation 1.1, the specific cutting force is an exponential curve fitting described with two constants, $k_{c1.1}$ and mc. The specific cutting force is vital during the calculation of feed force, torque, and power. It is a measurement of machinability for a specific material having a specific known chip thickness and rake angle. These force values are obtained from tables where the values are specific to various workpiece materials, rake angle, and chip thickness. The k_c value continuously decreases with the increase in the rake angle.

4. Result

The experiment was performed with seven different diameters on the drill bits and nine different feed rates. The model used to compare the test results in equation 1 is due to the significant factors changed in the experiment. Equation 1 considers both feed rate and the depth of cut (which is directly affected by the diameter) as significant factors, and so does the experiment set up, since the feed and diameter are the only factors changing.
Based on equation 1 a modeled result was calculated for the axial cutting force based on the experimental conditions and factors. The result from the experiment was not an exact match to the theoretical values. The error percentage between the measured and modeled axial cutting forces was calculated. the mean root square errors were calculated to provide the absolute value of the errors giving us the option to calculate the average error.

When analyzing the results, some patterns were detected. The first pattern is when the diameter increases, the error margin decreases. As visualized in Figure 2, there is a clear pattern that the absolute error decreases as the diameter increases. When the diameter is 2 mm, the absolute error is between 50-60%, but when the diameter is 16 mm, the absolute error is between 10-20%.

Another pattern is that increased feed leads to decreased error margin. Figure 3 shows the pattern. The variation can be caused by the difference in the diameter. If we compare the feed rate 0.1 and 0.22, the error margins for 0.1 are between 40-60%; meanwhile, the error margin for 0.22 is around 10%.

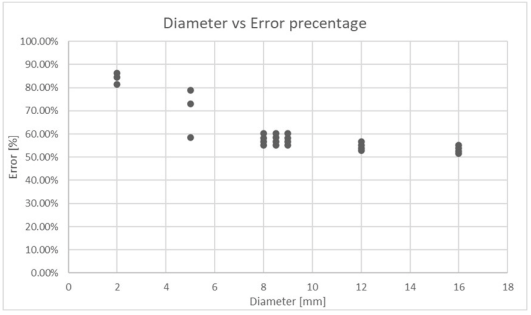

Figure 2: Correlation between diameter and error margin

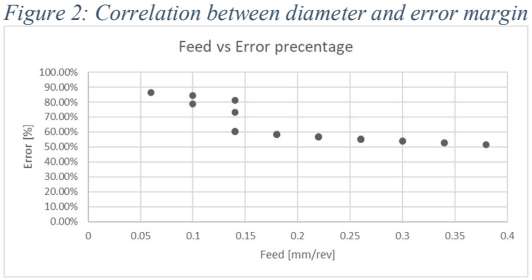

Figure 3: Correlation between feed and error margin

The next step in the project was to decrease the error between the measured and modeled axial cutting forces mathematically. The first numerical test was to affect the major factors by adding 2 exponential constants, one for the diameter and one for the feed rate, using solver calculation in Excel. The average absolute error decreased from 15.98% to 11.50%, the absolute max error increased from 55% to 56,89% and the absolute min error reduced from 0.33% to 0.23%. Where the exponential constant for the diameter became 1.08 and the exponential constant for the feed became 1.02.

To minimize the number of constants used in our optimization of the model, the next step was to try multiplying the original Equation.

The result of multiplying the model with a solver-based constant provided the least error between the measured and modeled axial cutting forces. The average absolute error decreased from 15.98 – 11.61%, with the constant being 1.127. The absolute max error went from 55% to 49.28% and the absolute min error increased from 0.33% to 2.83%.

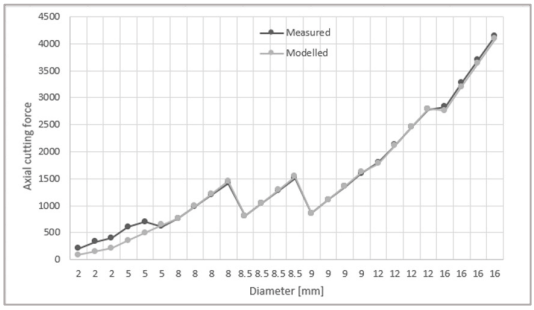

Figure 4: Correlation between the measured and modeled axial cutting forces focusing on diameter and feed after modification of the model with exponential constants.

After further modification of the model by adding both exponential constant and a product constant, the exponential constants balanced the differences in feed and diameter. The constant generated for feed was 1.19, the constant generated for the diameter is 1, and the constant for the whole model is multiplied by 0.83. The average error between the measured and modeled forces decreases to 9.42. Even with the improvement, the pattern on the small diameters and feed remained.

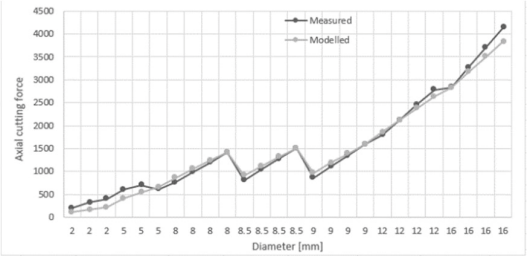

Figure 5: Correlation between the measured and modeled axial cutting forces focusing on diameter and feed after modifying the model with one constant.

The model can predict the axial cutting force for diameters bigger than 5 mm. This behavior will be analyzed in the next chapter. When removing the test results with a diameter of 2 mm, the error margin decreased even more.

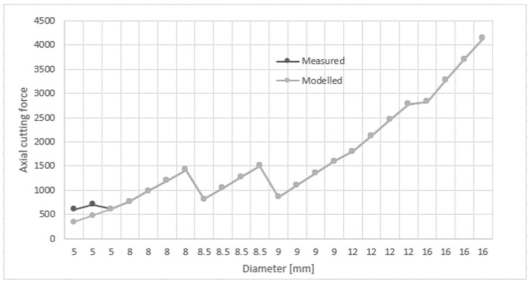

Figure 6: Correlation between the measured and modeled axial cutting forces focusing on diameter and feed after removing the test results with 2 mm diameter.

To see the variation in the absolute error between the bigger diameter, a graph was created from diameter 8 mm – 16 mm. When removing the test results with a diameter of 5 mm, the error margin decreased furthermore.

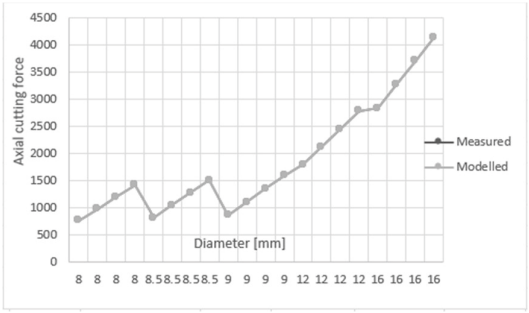

Figure 7: Correlation between the measured and modeled axial cutting forces focusing on diameters 6 mm - 18 mm.

5. Discussion and Conclusion

The significant factors that affect the axial cutting force in drilling operations are feed and tool geometry. In this project, an assumption was made that tool diameter and point angle is the most important factors but, as a result, showed later that the chisel edge ratio to diameter has an important role when it comes to smaller diameters. The difference in chisel edge ratio means that for future optimization of the model, the chisel edge ratio should be added into the model for better prediction of the axial cutting force with smaller diameters.

As shown in the equations above, increased depth of cut (a_p), increased specific cutting resistance (k_c), and high point angle leads to increased axial cutting force. In the original Equation, the increased feed would also lead to proportionally increased axial cutting force, but after the modification, the increased feed would lead to an exponential increase in the axial cutting force.

An empirical model that predicts the axial cutting force with less than 10% average error has been developed. This model is ideal for tools with a bigger diameter than 5 mm due to the lack of consideration of the chisel edge ratio in small diameters.

The model is underestimating the cutting force for the smaller diameters due to the difference in chisel edge. The model does not consider the different

ratios in tool geometry and tool profile. The chisel edge is significantly bigger in tools with smaller diameters to prevent tool breakage. Zhang, et al. (2015) described that the pattern seen in all the figures could be caused by the difference in the chisel edge ratio. The microscopic testing conducted confirms the of Zhang, et al. (2015) about the chisel edge ration increasing with decreasing diameter size. Since the chisel edge does not cut but push materials the bigger the chisel edge the higher the axial cutting force.

Additional to the chisel edge the β angle plays a significant role in axial cutting force. The smaller the β angle the sharper the cutting edge which leads to less axial cutting force. The β angle is not included in the model which can also be a factor that is creating the pattern with the smaller diameters. As shown in Figure 2 the smaller diameters have a higher range between the center and periphery β angles than the bigger diameters.

In summary, the final model is one with an exponential constant that balances the error difference by attacking the feed and with a constant for the whole model. This model does not work for smaller diameters due to the chisel edge ratio to diameter.

$$F_p = 0.834 * k_c * a_p * f_r^{1.196} * \sin k_r \qquad (2)$$

The optimized Equation is constant to the power of a_p, which is 1.003. The graph above explains the trend of varying errors if the constant varies. If the constant 1.003 is rounded to 1.00, then the error is increased from 9.42% to 9.87%. If the constants are further increased or decreased, the error margin is further increased, clearly seen from the graph below.

Equation 2 has a constant to the power of f_r, which is 1.196. The graph above explains the trend of varying errors if the constant varies. If the constant 1.196 is rounded to 1.2, then the error is increased from 9.42% to 9.95%. If the constants are further increased or decreased, the error margin is further increased, which can be seen from the graph. If the constant is replaced by a unit constant (f_r^1), the error remains higher, 31.36%.

Additionally, the Equation has a multiplication constant which is 0.834. The graph above explains the trend of varying errors if the constant varies. If the constant 0.834 is rounded to 0.8, then the error is increased from 9.42% to 13.13%. If the constants are further increased or decreased, the error margin is further increased, clearly seen from the graph. The influence of this constant is important. If the constant is removed (unit constant), the error would remain higher, 23.49%.

The model aims to provide minor errors to the maximum extend. The significance of constants is essential for the varying parameters in the Equation. Hence constants are applied for feed rate, diameter, and a multiplication constant for the entire Equation. The error margin is significantly higher if the constants are not considered 61.00%. The presence of error makes the model less realistic, and hence an optimized model is created to minimize the errors.

Moreover, if we consider the model errors, we can round off the constant exponential to ap, which is 1.003 to 1, making the error shift from 9.42% to 9.87%. There is no significant shift in the error, and the error margin is still less than 10%. Similarly, if we consider the other constant exponential to feed rate, the constant can be rounded off from 1.196 to 1.2, making the error shift from 9.42% to 9.95%. The rounding off the constants can only happen in terms of changing either ap or f_r individually. However, if both the constants are rounded off simultaneously, the error margin shifts from 9.42% to 10.43%.

On the other hand, rounding off the exponential constant of the depth of cut a_p would lead to the model having one less constant without any significant change in the error percentage between the measured and model axial cutting force. This insight leads to the final Equation without the exponential constant for the depth of cut. Equation 3 has an error percentage below 10%, which is acceptable according to the project's criteria and has one less constant than Equation 2.

$$F_p = 0.834 * k_c * a_p * f_r^{1.196} * \sin k_r \qquad (3)$$

To summarize, the project's final output is a mathematical model for predicting the axial cutting force in drilling operations shown as Equation 3. This detailed report on the process to achieve the model and a Microsoft Excel file with all the modified Equations and the result values are also the outcome of this degree project.

6. Acknowledgements

A special thank you to goes the people who have assisted us with valuable information and guidance throughout the work. Thank you for sharing your knowledge and thank you for your patience.

- Daniel Johansson, our supervisor from the Research and Development department in Seco.
- Andrii Hrechuk, our Co-Supervisor from the university, Ph.D.
- Professor Jan-Eric Ståhl, our Examiner.

Additionally, we would like to thank Seco Tools for their support with workpiece materials and tools and for providing experimental data.

References

Frezgi, H. & Gelli, B., 2021. *Axial cutting force in drilling operations,* Lund: Lund Universty.

Casting Simulation of Air Disc Brakes

Amalgamation of Simulation and Analysis results to achieve Parameter Mapping

Shankar V Patil, Shivakumar D Malagi

Department of Mechanical Engineering Sciences
Faculty of Engineering, Lund University
Lund, Sweden

ABSTRACT

Possibilities are immense when it comes to implementing Human ideas. Our aim was to combine results from Casting simulation and FEA of different components of Air Disk Brake, utilize these results to map parameters that affect the quality of Cast components to Structural analysis. The results obtained will also be used to improve castability and avoid expensive workarounds. The importance of the study can be emphasized by the fact that even after intensive simulations in FEA, unexpected failures occur during physical testing and, it is a well-known fact that physical testing is money and time intensive. With help of the results obtained through this study, the time and money invested in testing can be reduced, resulting in overall process improvement. Creo, Inspirecast, Nova Flow & Solid, Hyperworks, Ansys were the tools used to achieve the objectives. An opportunity to learn is an opportunity to grow. Learning new software like Inspirecast and Nova was challenging as well as rewarding. The project yielded useful results and improved our ken about Casting Simulation and FEA.

1. INTRODUCTION

Safety, dynamics, and durability are one of the most important parameters when it comes to heavy vehicles and their braking solutions. Haldex is one of the leading manufacturers in Brake and Air Suspension solutions. They specialize in creating innovative, efficient, and effective systems for the modern vehicles. A number of customers are mainly large manufacturers of trucks, buses and trailers in North America, Europe and Asia. Haldex also offers spare parts and servicing to distributors, workshops, and logistics companies. Haldex was founded in Landskrona in 1887 and has since been notable for ground-breaking technological vehicle solutions.

The background of the thesis topic – "Casting Simulation of Air Disc Brakes" deals with casted components which are rigorously examined in FEA before prototypes are ordered. Even after intensive simulations in FEA, unexpected failures occur during testing. The stresses indicated by the FEA are intermediate but are not expected to cause failures. The FEA uses a uniform material model and does not take varying material quality and casting defects into account. This leads to limitations in interpreting and using analysis results. This is exactly where the study comes into play.

1.1. Background

Liquified metal when poured into a cavity of desired shape with controlled as well as calculated flow rate and temperature, allowing it to solidify and cool down results in end products that have the required shape, dimensions, accuracy and properties. The finishing may not be as refined but additional machining can help address this problem. This process was first implemented all the way back in 4000 BC. Casting is one of the oldest documented process from the renaissance era. Thousands of years later, an unusual yet interesting factor led to development in this technique and that factor was religion. It may seem an odd and anachronistic reason but was influential in the development of Casting as metals like bronze were used to build Churches, Cathedrals and other establishments. It was not too late for people to notice this and utilize the technique for other areas of interest. Thus, the first Cannon was cast and as ironic as it may sound, it was a monk who made it happen.

Ever increasing development in computer aided technology has changed the course and the way in which the industries carry out their work. For instance, the design of a product or a component of a product was done manually by skilled, experienced engineers prior to the CAD era. This resulted in the requirement of skilled design engineer acquisition and even then, the process was time consuming, tedious and prone to errors. The introduction of Computer Aided Design software has been an immense blessing for basically any field of Engineering. Similarly, all the other engineering

processes which were carried out manually or based on trial-and-error methods in the past have been replaced with highly advanced as well as feature rich applications.

One of the many areas that underwent similar transition is Casting process. To understand the topic Casting Simulation, one needs to understand the terminologies and their meanings, the phases involved and the Science behind it. This will help an Engineer develop a profound and deep knowledge that will lead to rapid development over time and yield amazing results.

There are various steps involved in Casting Simulation right from Data gathering, Methods Design, Simulation, Optimization and Conclusion Report. There are several sub steps which involve CAD/CAM software like Creo, AutoCAD, Pro-E, Catia etc to form a solid 3D model of the Product, Gating system and other components as required, assemble them and save them in a file format that is compatible with the Casting simulation software. Once this stage is completed, the file is imported and processed to make it simulation ready. The Simulation setup has options to input values like temperature, flow rate, set material type, gating point, Filling parameters etc which will help in setting a simulation which is as close to reality as possible. After the setup is simulated, results like Porosity, Micro-Porosity, Shrinkage, Hot spots, Niyama, Brinell Hardness and others can be obtained that can be used to identify defects in casting and their possible locations.

1.2 Aim and Purpose

As stated in the introduction, the thesis report aims at utilizing the latest simulation software such as Nova Flow & Solid to perform casting simulations on Caliper and Carrier component of the Air Disc Brake model M115 manufactured by Haldex and employing the results obtained to find problematic areas that can be improved. Based on the results obtained from the simulations, mapping of mechanical properties such as yield strength, elastic modulus to structural analysis with the help of software like Hyperworks, Simlab and Ansys will be carried out. This may also lead to developing of plot results which combine material quality and structural loads to identify areas with low fatigue in the product.

Major part of thesis work involved developing, re-creating and modifying the existing gating system (developed by suppliers) for Caliper and Carrier, making minor modifications using CAD software CREO, saving it in a compatible file format for further simulations. Casting Simulation software is used for running simulation by providing inputs and setting the values of parameters such as Flow rate, pouring height in case of Gravity Casting, Adjusting the position of Gating points, Orientation of the product under cast and direction of the flow of Molten metal, as closely as possible to simulate real time casting environment.

Creating a workflow for setting up a generic casting simulation is one part of the thesis report. Upon completion of simulations, the results from simulation and Analysis will be mapped using Novastress (a feature in Novacast) and Ansys. The stresses calculated will be loaded on to a cloud of nodes of the component created using ansys and these nodes will be saved for result reading by importing them to Ansys or Hyperworks. The fishbone diagram maps major potential causes for casting defects. It is quite fascinating to see Raw materials, Person causes related to defects. These are the causes that are not immediately visible but have an impact in a way that is hard to trace compared to other causes.

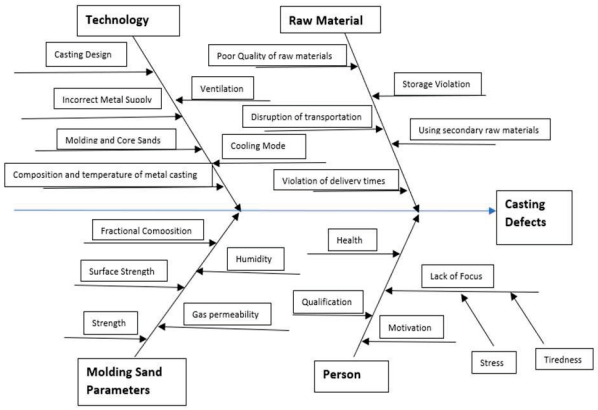

Figure 1.1: Diagram illustrating all potential causes for casting defects visually

2. METHODOLOGY

2.1. Gating system in CAD

The CAD 3D model of the caliper was used as a reference for replicating and building the gating system. Creo was employed for this purpose and the procedure started with selecting assembly as the working platform. Caliper model was imported by using the Assemble command. Building of the gating system was done by selecting the create component command in assembly window which lets you create a new component whilst still staying in the Assembly mode.

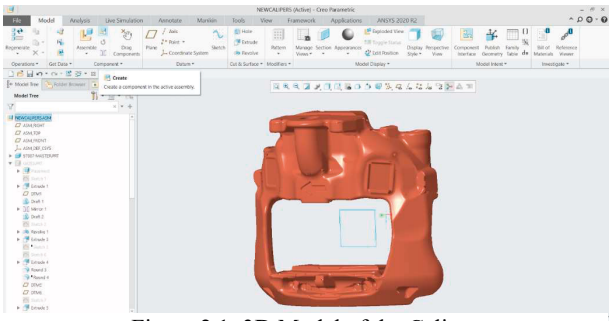

Figure 2.1: 3D Model of the Caliper

After selecting the necessary options and commands, the CAD design of the Gating System is created. In the design of Caliper gating system commands like Sketch, Spline, Arc, Extrude, Revolve, Project, Draft/ Taper, Round were used. The Riser which is similar to the shape of a wine glass was created using sketch, spline, revolve commands. Similar steps were carried out for design of Carrier gating system.

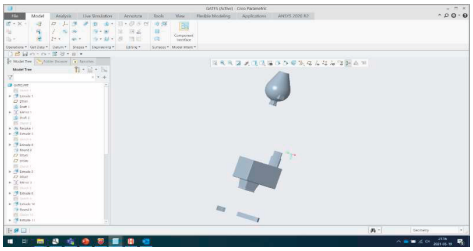

Figure 2.2: Gating system of the Caliper Isolated from the assembly

Upon completion of the setup in Creo, the file has to be saved in a format that is compatible for further processing. The file formats that are supported by majority of the Casting simulation software are STEP (.stp, .step) and STL (.stl). Saving the setup in either of the file formats in Creo marks the end of CAD processing phase of the simulation. It was found that the STEP files provide refined & smooth geometry when imported in the Casting Software when compared to STL files.

2.2. CASTING SIMULATION PROCESSING

The Simulation process begins with importing the previously saved STEP or STL file. The next step would be to fix the orientation in a way which reflects Iso view of the setup. Build Assembly would be the next option in sequence. Completion of this would result in a setup that has contact areas and a rigid build. Next step in the procedure is the Simulation setup. Options can be selected as required in this module where building of mesh, assigning of materials, temperature, gating point, setting up of Filling parameters and Shrinkage model can be performed. Adding of Vents, pins, chokes and numerous other options are also offered that can be implemented on demand.

The options for Simulation type are:

- Solidification
- Flow and Solid
- Flow Simulation

Based on requirement one can select one of the three. Flow and Solid simulation type was selected in this thesis report as it provided the results of both Solidification and Flow simulation. It did consume a significant amount of time when compared to only Solidification or Flow simulation for obvious reasons, but the results obtained were plenty informative. Figure 2.2 shows the gating system in creo and Figure 2.3 shows the first step in Novacast.

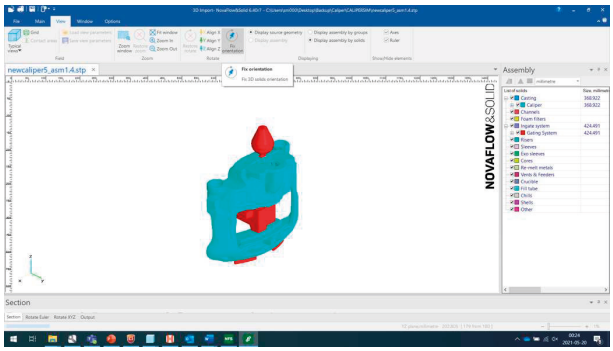

Figure 2.3: Novacast Import

3. RESULTS

The results obtained were informative and intriguing. As seen in the image below, the occurrence of shrinkage is in the regions closer to the edges. While most of the shrinkage is moved to the riser and mid-section of the gating system. This is acceptable because, during the machining process of the component the Riser and Gating are removed. The major function of Risers and Gating system is to eradicate Shrinkage or Porosity along with providing even solidification. In the 2D shrinkage defect image one can see shrinkages at various parts of the component. The shrinkage percentage is used to denote the chances of shrinkage appearing in practice when compared to simulation. If the shrinkage is 2 % or lower, then the possibility of it happening/ occurring in reality is slim. The Images seen in Figure 2 and 3 along with Figure 1 help in mapping the parameters. This is one such example of the many other type of results that can be mapped.

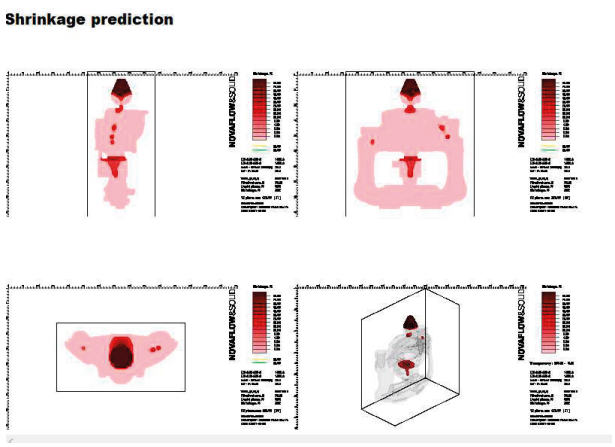

Figure 3.1: Shrinkage Indicator

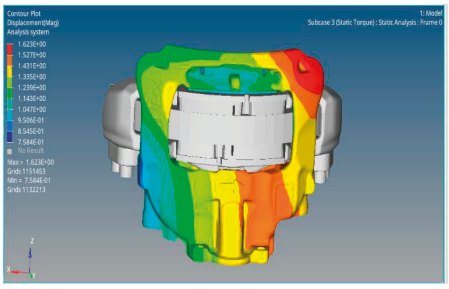

Figure 3.2: Static Torque

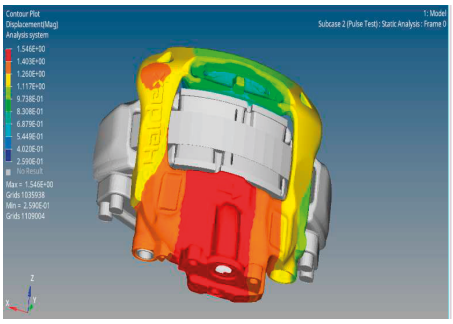

Figure 3.3: Pulse Test

From the images obtained above in Hyperworks, we can see the stress distribution for the Static Torque and Pulse test for the applied Load case.

4. DISCUSSIONS AND CONCLUSIONS

The results displayed that there is a possibility that the areas with Casting defects such as porosity are also the areas that have higher stress distribution in Finite Element Analysis results. The stress distribution although not fatal were intermediate but cracks were observed at those places in reality. Confirmation of this theory requires a lot more testing and simulation with varying combinations. In casting, room temperature cooling and solidification occurs with the inherent inhomogeneous distribution of the temperature which results in residual stress. The thinner regions within the lattice cool down more quickly and thus thermally contract, causing tensile stress. However, thermal stresses are alleviated by reduced output stress at high temperatures. When the temperature difference between faster and slower cooling rates is optimum, the maximum stress and plastic deformation occur. Compressive stresses occur in thin areas after complete cooling to a room temperature, while tensile stresses occur in the thick central layer. Hot tears can also be prevented by changing process parameters and cooling conditions or small adjustments to the casting geometry. Ductile Iron casting is considerably affected because of porosity. Cast quality has an impact on service life by taking predictions of defects such as shrinkage and porosity from casting simulation outcomes and transferring them to simulations for stress and fatigue. More detailed discussion and conclusion has been provided in the main thesis report [1].

ACKNOWLEDGEMENTS

We are grateful to Haldex for providing us this opportunity. The guidance and support were invaluable from Haldex Staff- Chief Engineer Mechatronics Design: Kristoffer Örndahl who is also the reason for this thesis to happen, Industrial supervisor and Calculation Engineer (R&D) at Haldex: Martin Wollstad and Senior Software Application Engineer at NovaCast: Erik Stivnert. Their immense experience and expertise helped us get over the obstacles. We specially appreciate the time and effort put in by Martin in guiding us throughout the thesis. His range of knowledge and ability to learn things is commendable.

We thank University Supervisor Aylin Ahadi and Per Hansson for their valuable inputs, guidance as well as suggestions. We also wish to extend our gratitude towards Jinming Zhou and Christina Windmark, LTH, Department of Production and Materials Engineering faculty for providing the knowledge, Support, Tools and information to be able to complete this report. Lastly, we sincerely appreciate the continuous and unparalleled support from our family for which we will be forever indebted.

REFERENCES

[1] *S. V. Patil and S. D. Malagi, "Casting Simulation of Air Disk Brakes," LTH, Lund, Sweden, 2021.*

Correlation between microstructural and mechanical properties in Niobium Carbide reinforced Hadfield steel composites

Lakshmi Manogna Dama

Department of Mechanical Engineering Sciences
Faculty of Engineering, Lund University
Lund, Sweden

ABSTRACT

Degradation of tools is a prevalent aspect in the mechanical world; due to the advancement of technologies and intense research and development, there are new ways and ideas to curb or delay the tool failures; one such idea is to implement Metal Matrix Composites (MMCs) with various reinforcement materials. This thesis focuses on improving the hardness and wears resistance of the Hadfield steel by reinforcing them with Niobium Carbide (NbC). The results from this study have shown an increase in hardness and wear resistance of the studied composites.

1. INTRODUCTION

Among steels, Hadfield steels also commonly known as Manganese steels have remarkable properties, the main reason behind their usage in mining industry is because of their work-hardening property, hence they are very widely preferred in crushers liners. But however, over a period of time they fail too. The important concept behind this project is to increase the hardness of manganese steel by reinforcing it with Niobium carbide.

2. METHODOLOGY

The thesis began with an intensive literature review on Metal Matrix Composites (MMCs), Hadfield steel, Niobium carbide etc., The experimentations involved microstructural analysis performed under optical microscopy and Scanning Electron Microscopy (SEM). Mechanical testing was performed using a Vickers Hardness tester. Finally, wear resistance was calculated by performing lab wear test.

A total of 14 compositions are planned, but due to challenges faced during the thesis and also due to COVID restrictions only 11 of them could have been made.

2.3. ANALYSIS AND DISCUSSION

Due to time constraint only four samples have been analyzed under Scanning Electron Microscopy (SEM), and the results have shown that there are microscopic pores due to casting defects, and few samples had cracks which have been developed due to thermal stresses during heat treatment and quenching. Other than that, all the analyzed samples had good bonding between MMC and base alloy. Later micro hardness test has been performed on the samples and it has been observed that the hardness of the reinforced region is relatively higher than the hardness of the base alloy region. Finally wear test has been conducted. Due to time constraint only one sample has been tested for wear. It has been found that there is significant improvement in wear resistance in the studied sample.

3. CONCLUSION

- The correlation between microstructural and mechanical properties have been drawn and found that the particle size is proportional to hardness
- The EDS analysis have confirmed the microstructural homogeneity of NbC particles.
- Microstructural analysis has shown the samples have resulted in different particle size reinforcements, which indeed impact the overall hardness.

4. FUTURE SCOPE

- Due to time constraints, only four samples were analysed in SEM. Hence the remaining samples should be further analysed.

- Another vital aspect is XRD analysis; due to limited access, this analysis could not be carried out; hence, it is highly suggested to carry out XRD analysis

ACKNOWLEDGEMENT

To **Dr. Latifa Melk**, I appreciate the kind of dedication that she has towards her work and her students; I would like to thank her for giving me an excellent opportunity to work with **Sandvik Rock Processing Solutions;** her supervision and suggestions have always guided me towards the right direction and final gratitude for having trust in me that I would finish this project.

Special thanks to Hema and Manideep for their assistance throughout the project.

REFERENCES

[1] Manogna D. L., 2021; Correlation between microstructural and mechanical properties in Niobium Carbide reinforced Hadfield steel composites, LTH, Lund University, Sweden.

Development of Optimized Cost Models for Recycling and Remanufacturing.

A step towards the circular economy

Abbu Spuran Reddy, Badri Reddy Gade

Department of Mechanical Engineering Sciences
Faculty of Engineering, Lund University
Lund, Sweden

ABSTRACT

Resource consumption is rapidly increasing with enormous population growth. The current linear economy model is unsustainable in the way it operates. A new approach such as a circular economy is required to preserve the resources and reduce the environmental impacts. This research emphasizes increasing recycling and re-manufacturability through an economic model and helps stakeholders make better decision-making.

1. INTRODUCTION

In today's rapidly changing global economy with the context of resource consumptions and decreasing resource supply, numerous concerns have been raised to meet the demand for future generations. We adopted a linear business model to meet our present needs, also described as the ¨take-make-dispose¨ model. With this model, we extract raw materials and transform them into a product as economical as possible and use them for a while. When the product loses its functional and economic value, they are disposed as waste. Due to this, there are shortages in critical supplies of resources, and other critical raw materials will be exhausted soon. And other consequences include the destruction of natural resources such as forests and lakes, toxic emissions, fluctuating commodity prices, increased demand for materials, geopolitical dependencies, or biodiversity loss. To encounter all these adverse effects, a concept of circular economy **(CE)** has been introduced. The primary aim of CE is to extend the product life or materials either by keeping them in the stream as much as possible or by bringing them back into the stream after their end of life **(EOL)**. Generally, the product/material that lost its functional and economic values is considered as waste. In CE, this waste will be processed to bring the disposed products into use or recover the disposed products' material. To obtain the materials back to the mainstream, approaches such as recycling and remanufacturing have been incorporated in CE.

Several authors have conducted several studies on recycling and remanufacturing but, there have been very few economic models for calculating the cost of recycling and remanufacturing. The existing models are the summation of various direct costs involved in the recycling and remanufacturing processes. But none of these models have explained about various activities involved in recycling and remanufacturing processes, important resources required for various activities, and technological factors related to the processes. Also, from Sopel's assessment, it was found that, even though millions of tonnes of metals are currently recovered and used each year globally, even more metals can be recovered if an appropriate economic model is presented. To fill this gap, this study will focus on identifying the major activities involved in recycling and remanufacturing processes, important resources required for various activities, and technological factors related to the processes. Based on the findings, economic models are developed for calculating the cost of recycling and remanufacturing.

2. METHODOLOGY

Case research methodology is used in this study to form a research framework and determine the hypothesis of the research. Qualitative data is the primary source of data collection. The data is gathered from various academic literature and industrials resources. From various resources, multiple cases have been studied in order to ensure the reliability of the model. The data analysis was performed on the key findings from the individual resources in order to address the research hypothesis. The quality of the research is validated using constructive validation. In search of the literature, various keywords are used to refine the articles.

2. THEORETICAL FRAMEWORK

The economic models developed for calculating the cost of recycling and remanufacturing are based on an activity-based cost accounting **(ABC)** model and a basic economic model for judging production development. Like the ABC model, these developed models focus on identifying the major activities involved in recycling and remanufacturing and then determine the resources involved in each activity. Then an appropriate cost driver (for ex. Cost/hour) is selected for every resource. Then the cost of the resources is coupled with technological factors related to processes as explained in the basic economic model for judging production development. In this way, these developed models help in calculating the costs associated with a particular activity, calculating the overall cost of recycling a ton of material, and the cost of remanufacturing per product. Also, these models consider technological factors (like production rate losses, downtime losses, setup time, etc.), which form the basis for decision-making in product development.

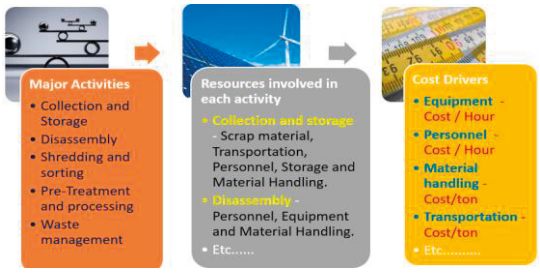

Figure 1: Example of application of ABC model principle for recycling process

4. RESULTS

This section presents the various activities involved in recycling and remanufacturing processes, important resources required for various activities, technological factors related to the processes, and the economic models for calculating the cost of recycling and remanufacturing.

4.1. MAJOR ACTIVITIES IN RECYCLING AND REMANUFACTURING.

Table 1: Major activities in Recycling and Remanufacturing Processes.

Recycling	Collection and Storage, Disassembly, Shredding and Sorting, Pre-treatment and processing, Waste Management.
Remanufacturing	Disassembly and Cleaning, Inspection, Machining and Material Addition, Inspection, Assembly, Functional Testing and Painting.

4.2. MAJOR RESOURCES, COST DRIVERS AND TECHNICAL FACTORS ASSOCIATED WITH RECYCLING AND REMANUFACTURING.

Figure 2: Resources involved in Recycling and Remanufacturing.

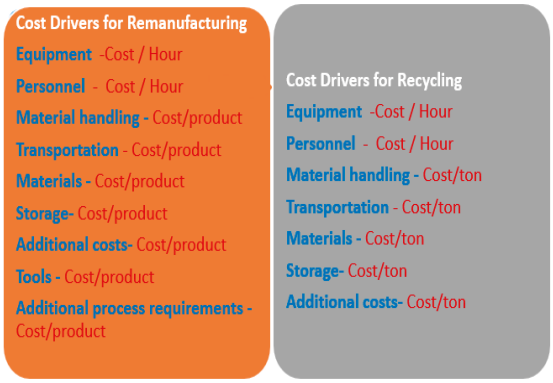

Figure 3: Cost drivers

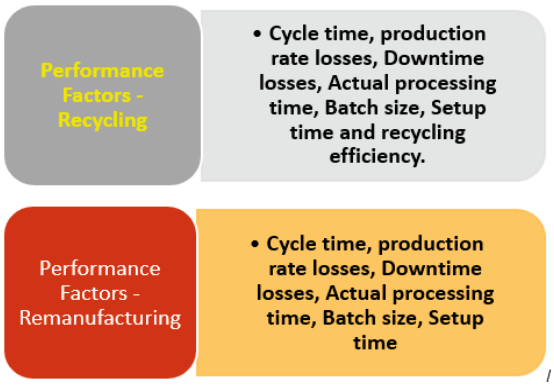

Figure 4: Technical or performance factors Involved in Recycling and Remanufacturing

$K_{Materials}$ = cost associated with direct and indirect materials.
$K_{Equipment}$ = cost associated with all the processing equipment involved in all the activities.
$K_{Personnel}$ = cost associated with all the personnel involved in all the major activities.
$K_{Material\ handling}$ = cost associated with material handling systems involved in between all the activities and in between the various activities and storage.
$K_{Transportation}$ = cost associated with transportation involved in activities 1 and 5.
$K_{Storage}$ = cost associated with storage involved in various activities.
$K_{Additional}$ = cost associated with quality assurance, health and safety and any activity based indirect costs.

4.3. EQUATIONS FOR CALCULATING THE COST OF RECYCLING PER TON OF MATERIAL

As per the ABC model, the cost of recycling ($K_{Recycling}$) can be calculated by adding the cost associated with all the activities involved in the recycling process.

Therefore,

$$K_{Recycling} = K_1 + K_2 + K_3 + K_4 + K_5 + K_{Material\ handling} + K_{Transportation} + K_{Additional} \quad \text{(Eq. 1)}$$

Whereas
K_1 = costs associated with the collection and storing activity.
K_2 = costs associated with disassembly activity.
K_3 = costs associated with shredding and sorting activity.
K_4 = costs associated with pre-treatment and processing activity.
K_5 = costs associated with waste management activity

From the above equation, we can calculate the cost of recycling per ton by calculating the costs associated with every activity involved in recycling. Suppose one would like to focus on the costs associated with a particular resource group, like the total cost of materials or the cost of total equipment involved in the recycling plant. In that case, the cost for recycling a ton of the material can be calculated by using equation 2.

$$K_{Recycling} = K_{Materials} + K_{Equipment} + K_{Personnel} + K_{material\ handling} + K_{Transportation} + K_{Storage} + K_{Additional} \quad \text{(Eq.2)}$$

Whereas

4.4. EQUATIONS FOR CALCULATING THE COST OF REMANUFACTURING PER PRODUCT

Just like recycling process, by applying ABC model principle, the cost of remanufacturing per product can be calculated as

$$K_{Remanufacturing} = K_1 + \sum_{i=1}^{Z} K_2 + K_3 + K_{Material\ Handling} + K_{Storage} + K_{Additional} \quad \text{(Eq. 3)}$$

Whereas
K_1 = the cost associated with stage 1.
K_2 = cost associated with stage 2 for a specific part type.
K_3 = cost associated with stage 3.

- Disassembly activity falls under stage 1
- Cleaning, Inspection, Machining and Material addition falls under stage 2.
- Assembly, Functional Testing and Painting falls under stage 3.

If one would like to focus on the costs associated with a particular resource group (like the total cost of personnel or the total cost of the equipment involved in remanufacturing plant etc.), then the total cost of remanufacturing per product can be calculated by adding the costs associated with each resource group similar to equation 2.

5. DISCUSSIONS AND CONCLUSION

a. The consideration of performance or technological factors in every activity helps in monitoring the ongoing production to identify the areas that need improvement. This

consideration also forms a basis for the decision-making during process or production development in the identified areas.

b. The model developed for the recycling process also considers the cost associated with various kinds of material losses involved in various activities by considering x_{in} and x_{out} in every activity. Similarly, the model for remanufacturing also considers the cost associated with rejected parts and new parts added to the product. These considerations make these models even more precise.

c. The recycling efficiency considered in pre-treatment and processing activity helps in using the model for various metals. Because various metals will have various recycling efficiencies and, in this model, the recycling efficiency is coupled with the Output of the recycling facility. Change in recycling efficiency will affect the Output of the recycling facility. We know that the Output of the recycling facility plays a crucial role in the cost of recycling.

d. Similarly, there are several advantages and possibilities with these developed models, as explained in sections 6.2 and 6.3 in the thesis report.

In conclusion, this thesis has pursued insight into the current recycling and remanufacturing economic models. It has been found that these industries are gaining traction with an increase in resource consumption and depleting natural resources. Due to the rapid change in industries, new economic models are required to change how the business is being carried out within resource management. Moreover, the findings in the literature survey suggested that more economical models are required to improve the product and material recovery. Based on the key finding, in this thesis, we have developed the economic models for recycling and remanufacturing. In addition to calculating the cost of recycling and remanufacturing, these models also help in making decisions when it comes to production development.

6. LIMITATIONS OF THE MODELS

- The annual demand for recycled material or remanufactured products plays a crucial role in selecting the batch size, which affects the cost of recycling and remanufacturing. In most situations, the annual demand is uncertain. These developed models for recycling and remanufacturing haven't considered the uncertainty of demand.
- The developed equation for calculating the cost of recycling is only applicable for metals.
- The equation for calculating the cost of remanufacturing is only applicable to original equipment manufacturers (OEM's) and contracted (outsourced) remanufacturers. This model does not apply to local remanufacturers.
- These developed models contain several numbers of parameters. To get more accurate results, these models demand well-structured data.

7. FUTURE SCOPE

- Adaptation of recycling model for various materials.
- Adaptation of remanufacturing model for various types of re-manufacturers
- Considering the uncertainty of data in the model.
- Adopting dynamic simulation in order to reduce the complexity in the requirement of well-structured data.
- These developed models can also be adopted for price quoting purposes.

8. ACKNOWLEDGEMENT

First of all, we express our deepest gratitude to our supervisor, Christina Windmark, who has been supportive with her guidance, comments, and continued motivation throughout our master's journey and this thesis. We thank her for trusting and believing in us. Working with her, we have learned and adapted various nuances and facets of professional life in Production Systems. We could not have asked for more dedicated and helpful tutors. We are incredibly thankful to our parents, family, and friends. We thank them for believing in us and always being a source of encouragement and positivity. Special mention to our parents for being emotionally strong and proud of us. Finally, we would like to thank each other for being there during the most uncertain times and pushing each other to go the extra mile to accomplish what we started.

9. REFERENCE

[1] Reddy, S. & Reddy, B., 2021. *Cost Models for Recycling and Remanufacturing- A step towards circular economy*, Lund: Lund University.

Different Heat Treatment parameters investigation on microstructure, mechanical and wear properties of Hadfield Steel

Rahul Milind Kulkarni, Vishwajit Vishnu Kolekar

Department of Mechanical Engineering Sciences
Faculty of Engineering, Lund University
Lund, Sweden

ABSTRACT

Hadfield Steels make up a significant group of steels that can perform with their higher strength, excellent wear resistance, and good formability. To achieve this distinctive behavior along with the alloy compositions, heat treatment is also a vital factor. Alloy carbides can be controlled with various heat treatment techniques, as they directly affect the loss in strength, which eventually leads to making the material more ductile. The changing times require all the materials to be more efficient from all the perspectives one could ever imagine. The steel industry must continue to look into the introduction of unique heat treatment techniques. The current study examines the microstructure and mechanical characteristics of three different (compositions) Hadfield Steels, after the implementation of different heat treatment cycles along with an aqueous quenching medium, in this frame of reference. To complement this experimental work, an extensive literature review has been carried out to foresee the outcomes. This study reveals that Steels X, Y, and Z have finer grain boundaries, and show its tendency towards the optimal hardness values, when heat treated with the new Heat Treatment Cycles. To sum up, this is a wide area to explore, and all the small details with respect to the heating and quenching play a crucial part in the development of the heat treatment cycle and so the Hadfield steel.

1. INTRODUCTION

In this day and age, Hadfield Steel is the material of choice to be used in crushing applications. During the process of Hadfield steel, heat treatment (HT) is considered as a crucial step since the annealing temperatures have a strong effect on the mechanical properties, hence the wear resistance. Therefore, there is a strong interest in understanding the effect of HT parameters, the properties of Hadfield Steel.

Sir Robert Hadfield discovered Manganese steel/Hadfield steel in the year 1882. This type of steel is also known as Mangalloy. This type of steel is High alloy steel with a Carbon content ranging from 1.1%-1.4%, and the Manganese content ranges from 11%-14%. This type of steel is unusual because it blends good strength and ductility with such a good vulnerability for work-hardening and strong resistance to abrasion.

Because of the Hadfield Steels high C and Mn content, their cast structure comprises of austenite grain with carbides dispersed in the grain borders. This type of structure is brittle as well as often ineffective. Fast quenching of Hadfield steel after austenitization heat treatment in a salt bath can prevent grain boundary carbides accumulation. Its structure in the form of casting contains carbide phases such as $(Fe,Mn)_3C$, on which a complete austenitic structure can be formed with adequate heat treatment. The austenitic single phased microstructure will be formed after an austenitizing and quenching heat treatment. The specified alloy will achieve the required hardness through heat treatment. The implementation of heat treatment results in the appropriate mechanical properties. As a result, the dissolving temperature must be high enough to dissolve the carbides in austenite. To achieve a supersaturated matrix, rapid quenching of the austenite's single-phase structure is essential. And this is where the study comes in.

1.1 OBJECTIVE

This thesis aims to study and investigate the effects of various implemented heat treatment cycles for the existing Hadfield Manganese steel grades X, Y and Z with improved microstructure and mechanical properties. The study will provide insight to new heat treatment cycles, as well as various quenching methods to give a better interpretation.

The key emphasis is to study the microstructural evolution of these steels subjected to various heat treatment cycles. The aim is to lower the carbides and improve grain boundaries which will further improve toughness without affecting other properties such as mechanical and microstructural analysis. The literature study can also be used to visualize out every variety of heat treatment methods. Therefore, this study employs a multidimensional approach that includes experimental

and analytical elements to determine logical and quantitative growth alternatives and then improve understanding through estimating the consequences of improvements in the manufacturing of the Hadfield steel, especially from the point of heat treatment.

2. METHODOLOGY

Heat treatment Processes (HT-1,2,3,4,5) for X, Y, and Z grades have been performed. Further, all samples were cut into the desired dimensions for heat treatments. All samples were subjected to different material characterization techniques. At first, Optical Microscope (Alicona) was used to examine the microstructural in low magnifications, Then, Scanning Electron Microscope (SEM) was used to analyse in depth the formation of carbides in the grain boundaries, Finally, Elemental Dispersive Spectroscopy (EDS) was used to examine the composition of different carbide formed. The mechanical properties such as hardness has been tested after each heat treatment cycle.

3. RESULST AND DISCUSSION

It has been observed that the different heat treatment cycles have resulted in low carbides formation in the grain boundaries. Carbides were present because there is an abundance of C and carbide-forming elements like Mn and Fe. Due to the high amount of C and Mn content, the presence of austenitic matrix is observed. Carbides within the matrix, especially $(Fe\ Mn)_3C$ type carbides, carbides along or around the grain boundary, spherical or rod-type carbides, and eutectic carbides, are the types of carbides that impact the performance of Hadfield steels. The experimental heat treatment (HT1) gives the fine-grain boundaries for all the three steel grades (X, Y, Z). Steel grade Z showed delicate grain boundaries than X and Y, which means it has a lower amount of carbide present on grain boundaries as well.

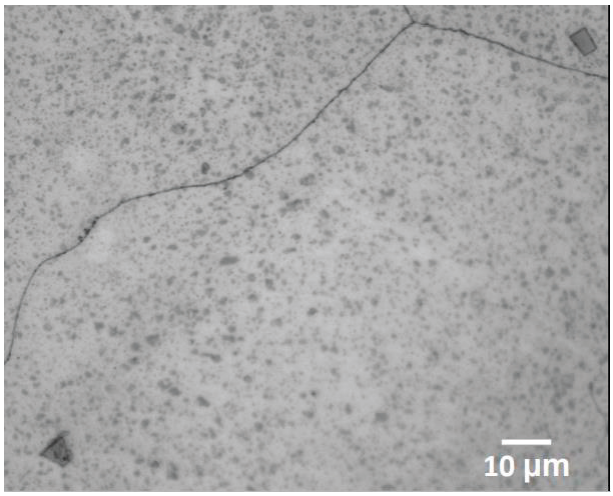

Figure 1: Microstrue of Steel grade X, after the heat treatment process – 1.

As in an austenitic matrix, a lower carbide content indicates more Carbon is dissolved in the austenitic phase When the average hardness of sample X, Y, Z samples is compared, it was found that the heat-treated Z grade sample has the maximum hardness, but the difference between it and the other two grade samples X and Y, is negligible.

The experimental heat treatment HT2 result quenching in salt solution of all three grades shows connected carbides on grain boundaries as well as dispersed carbides in austenitic matrix. However, the amount of carbides present is much lesser than as quenched in higher salt solution. This is because salt has a higher quenching rate compared with pure water. When the average hardness of X, Y, Z samples are compared, it is found that the value of all three samples was close enough further, resulting in reaching optimum value.

For the heat treatment (HT3), a dispersed carbide in grain boundary was obtained. In the Z grade sample, there was a homogenous distribution of carbides in the austenitic matrix when compared to a sample of grade X and Y. Moreover, the hardness of sample grade X is higher than that of Y and Z due to the presence of carbides in the austenitic matrix.

Heat treatment HT-4 shows the minute number of carbides present in grain boundaries. Samples of grade Y and Z which were processed by this heat treatment, did not appear to have any carbide. This is because, when the material is heated to austenitization temperature, the entire structure turns into 100% austenite. The quick cooling was carried out to avoid carbide reformation. The hardness value of sample grade X is higher than the other two sample grades. The reason may be due to the presence of carbide both at the austenite grain boundaries and in the matrix, as seen in the microstructure of the

tempered sample. Using water and aqueous salt solution as quenching medium for various austenitization temperature the carbide formation along the grain boundaries have been reduced.

4. Conclusions

Heat treatment 1, Heat treatment 2 with lower salt content solution, Heat treatment-3, and Heat treatment-4, provides good microstructure as well as optimum hardness for high Hadfield steels.

4.Acknowledgements

We would like to express our deep sense of gratitude towards Sandvik SRP for providing us with the opportunity and funding to carry out this thesis. It has been a great privilege and honor to be associated with this company. This thesis would not have been possible without the help, support, and patience of our supervisor Dr. Latifa Melk. Also, we would like to thank Jörgen Petersson, Foundry Specialist, Sandvik SRP, for his valuable insights and the rest of the company for assisting us directly or indirectly.

We would like to mention special thanks to Jan-Eric Ståhl, and the Division of Production and Materials Engineering. They got us the opportunity to write our master thesis at such a large and respected Swedish corporation. They helped us by providing all the necessary support to complement this thesis.

5.References

Kolekar, K. a. (2021). Different Heat Treatment parameters investigation on microstructure, mechanical and wear properties of Hadfield Steel.

Experimental study of surface integrity in drilling Inconel 718 with uncoated and PVD coated tools

Shao Du

Department of Mechanical Engineering Sciences
Faculty of Engineering, Lund University
Lund, Sweden

ABSTRACT

In the manufacturing industry, drilling is a commonly used process for making holes for the components. The surface integrity of the holes is very crucial to the function and performance of the component. Cutting tool material and cooling conditions in the drilling process have a significant impact on the surface integrity of the drilled surface. The aim of this project is to experimentally investigate the effect of coating materials and cooling condition of the drill bits on the surface integrity of drilled hole in the drilling of Inconel 718 alloy. Three drill bits were used in the experiment tests in drilling the Inconel 718 to investigate the surface integrity of the drilled surface. Tool life, tool wear, feed force, radial force and torque variations were measured during the experiment. Then, surface integrity was characterized, including measurements on surface roughness and thickness of material drag layer. Study also includes the diameter variation and burr on drilled holes. The conclusions show the PVD coating on the drill bit extends the tool life by improving the wear resistance and provides better surface quality of the machined surface. Moreover, the drill bit with four cooling channels instead of two has better cooling performance, leading to less flank wear of drill bits to extend the tool life. More tests about surface integrity can be conducted for future work like a residual stress test, nano-indentation test.

1. INTRODUCTION

Used for the aerospace sector like jet engines, Inconel 718, as one type of nickel-based superalloys. Inconel718 has properties of higher oxidation resistance and high-temperature strength to make sure it retains the properties and works in an extreme environment at high temperature and high pressure [1]. For Inconel 718, the properties of high abrasiveness, high hardness, low adhesion, high strain hardening and low thermal conductivity make it a low machinability material [2]. So, the cutting tools need to be hardened, tough enough and have good wear resistance to machine Inconel 718. Besides, surface integrity determining the functionality, longevity and performance of the workpiece is investigated. Surface integrity includes the superficial surface and subsurface of machined workpiece on the microscale. How the cutting tool material and cooling conditions in the drilling process affect on the surface integrity of the drilled surface will be investigated in this project.

2. RESEARCH METHOD AND EXPERIMENTAL DETAILS

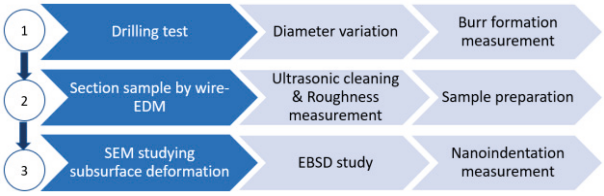

Figure 1: Illustration of research method

Figure1 illustrates overall research method applied in this study. Due to the time limitation, the ESBD study and nanoindentation measurement will be conducted in the future.

2.1. DRILL TEST

Inconel 718 is used as the workpiece to be drilled. The Inconel 718 workpieces were in the shape of a round bar from hot forged with the treatment of solution annealed, aged and peeled condition. The workpiece has a diameter of 115mm, and a height of 42mm. The tensile strength is 916 MPa. The yield strength is 878MPa and the hardness is 45 HRC.

Three types of cemented carbide drilling tools with and without coating, two and four cooling channels were used in the current study. Tool Ref represents the reference tool, which is uncoated with two cooling channels. Tool A and tool B represent the PVD coated drills by the same coating materials with multi-layered coating. Tool Ref and Tool A have integrated with two coolant channels, while Tool B has four coolant channels. The drilling test was conducted on Mori Seiki NV5000 α1 machine. Kistler sensor was used for measuring cutting forces and torques during the drilling test. Zeiss microscope was used for wear measurement and taking photos. Data analysis were conducted by the software DASY Lab. The diameter of three twist drill bit is 8.5 mm. the total cooling channels area for all three drill bits are similar which are 3.1 mm^2. The cutting speed is 25

m/min, feed rate is 0.1 mm/rev. the coolant is 7.0% with 45 bars. The end of tool life is treated as the flank wear reaching 0.2 mm.

2.2. SAMPLE PREPARATION

- Wire-EDM

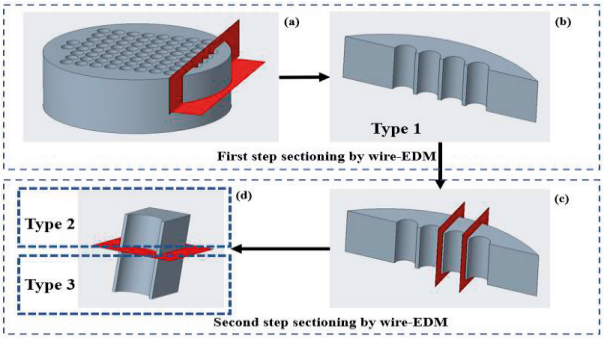

Figure 2: Schematic drawing of the workpieces sectioning by Wire-EDM. Step 1: (a) The workpiece was cut to (b) get the strip with cross-sectional holes; Step 2: (c) The specific hole was cut again (d) to be in two parts.

For further investigation of the surface roughness, microstructure and subsurface of the drilled holes, the workpieces were cut using wire-EDM, Brother HS-5. Cutting was done in two steps. The first step of cutting was to get the cross-sectional holes in strips as Type 1 in Figure 2 (b) from the workpiece in Figure 2 (a). Strips in Type 1 were used for measurement of surface roughness by light optical microscopy. Based on the first step of cutting shown in Figure 2 (b), the second step was to get the two parts of the specific hole as shown in Figure 2 (d) for further microstructural analysis. After this step, parts like Type 2 & 3 got from Type 1 in Figure 2 (d).

- Mounting, polishing, and grinding

In this project, mounting provides convenient handling of small specimen, which is helpful for the mechanical preparation later. Cito-press-5 is used for hot mounting. AntiStick is the mould release agent to the rams of mounting presses, which is used before placing the specimen. Polyfast is used as the resin to provide high preparation quality and short process time. After hot mounting, mechanical preparation takes the main part in this section, including grinding and polishing. After grinding and polishing, to improve the specimen surface quality, the specimen is polished again in a vibration polishing machine Pace technologies, giga-1200 vibratory polisher during 14 h using OP-S, 0.25 µm suspension. At last, the specimens were immersed in ethanol and cleaned by ultrasonic device Branson-2510. The steps for grinding and polishing are following below: SiC foil to remove the plastic; MD-Largo 9 to remove big scratcher; MD-Dac 3; MP-Piano 1; MD Chem.

2.3. LIGHT OPTICAL MICROSCOPY

After finishing the drilling test, several parameters can be measured prior to sectioning by wire-EDM—for example, the diameter of drilled holes, the height and the width of the burr. The cross-section of holes was used to measure the surface roughness of selected drilled holes. All these measurements were conducted by using a light optical microscopy, 'Alicona Infinitefocus G4' with 'MeasureSuite 5.3' software.

3. RESULT AND DISCUSSIONS

3.1. TOOL LIFE

For the uncoated tool Ref, there are a total of 44 holes have been drilled before reaching the end of tool life (VB=0.2 mm). For the coated tool A with two cooling channels, 140 holes are drilled. For the coated tool B with four cooling channels, 210 holes are drilled. Table 6 shows the list of drilled holes selected for measurements of flank wear, feed forces, radial forces and torques.

- Tool wear

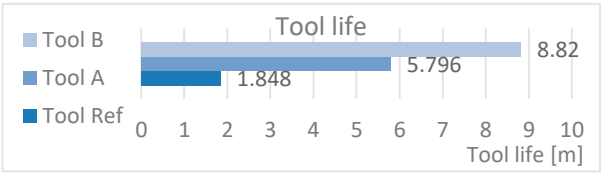

Figure 3: Comparison of tool life for three drill bits

Figure 3 displays the tool life of studied drill bits (values were converted to cutting length from hole number). Comparison of the tool life of tool A with two cooling channels and tool B with four cooling channels, the tool life of tool B is roughly 50% longer. When comparing the tool life of uncoated tool Ref and coated tool A and B, the application of coating extends the tool life significantly.

3.2. CUTTING FORCES

- Feed force

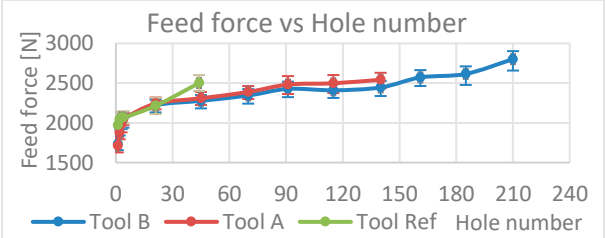

Figure 4: Comparison of feed force vs number of drilled holes for three drill bits

The feed force increases with the increase of the number of drilled holes for all investigated drill bits, as shown in Figure 4. The uncoated drill bit has a higher feed force on drilling the first hole compared with the other two coated drill bits. However, with the rise of the

number of drilled holes, the feed forces for tool A and tool B are similar and constantly increasing until tool A reaches the end of its tool life on hole number 140. Simultaneously, the feed forces on tool B are lower than the feed forces on tool A. From hole number 140 to 210, the feed forces on tool B increase at a higher rate. Figure 5 shows the general torque development with increasing the number of drilled holes. In Figure 6, the radial forces from hole number 1 to 4 by tool A are higher than two coated tool A and tool B. After hole number 20, the radial forces by three drill bits are close on the same number of holes. Besides, the radial forces are relatively stable.

- Torque

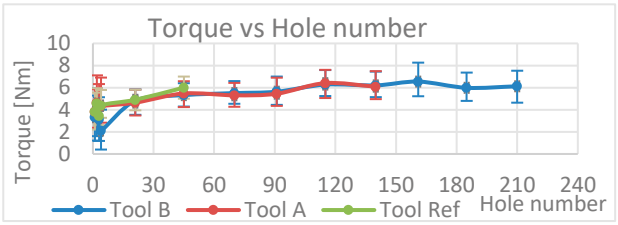

Figure 5: Comparison of torque vs number of drilled holes for all studied drill bits

- Radial force

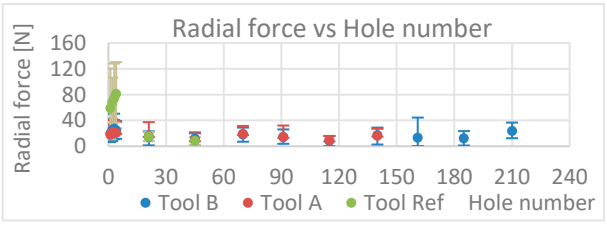

Figure 6: Comparison of radial force vs number of drilled holes for all studied drill bits

Start comparing with tool Ref and tool A, the coated tool A takes the lower feed force at the beginning of four holes, then, the values of feed forces gradually become closer. A similar tendency was found when studying the radial forces. However, the differences in radial forces for tool Ref and tool A increase until hole number 20. Based on these findings, it can be explained that the smooth surface of the coated layer and the sharper cutting edge of the coated drill bit gives the lower feed and radial forces at the beginning of drilling. When comparing coated tool A and tool B, most of time, the tool B with four cooling channels takes the lower feed and radial force, which means that four cooling channels improve the cooling effects and leading to decrease of flank wear and subsequently longer tool life.

3.3. DIAMETER VARIATION

Figure 7 shows the comparison of diameter variation with respect to hole number among three drill bits; the result was obtained by the image processing [3]. Tool A and tool B have a larger diameter at the beginning of drilling due to the presence of coating. Besides, the diameter of drilled holes tends to decrease with increasing the number of drilled holes regardless type of used drill bit. When the drill bit is worn out, the actual diameter of the drill tip becomes smaller than the fresh drill. Tool B has a smaller range of diameter variation compared to tool A, which means that tool B has better wear resistance. Comparing tool Ref and tool A. The coated drill bit has a high range of diameter variation due to higher drilling length and the BUE on the edge of tips. To compare tool A and tool B, the drill bit with four cooling channels has a lower range of diameter variation. It can be due to the good cooling property leading to less tool wear and the chippings on the tips.

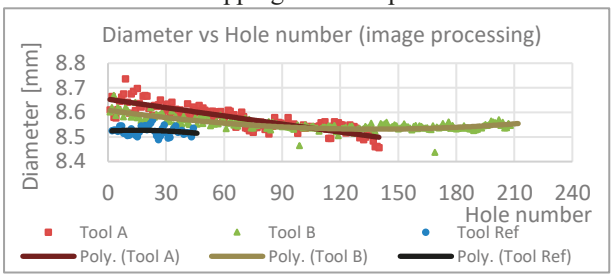

Figure 7: Diameter variation VS hole number for three drill bits by image processing

3.4. BURR

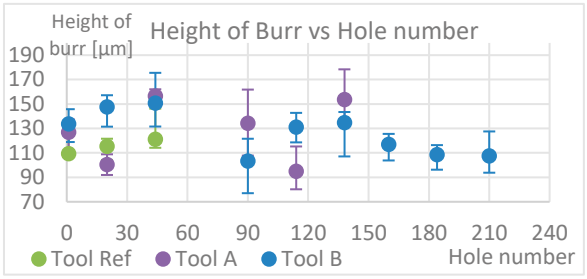

Figure 8: Comparison of the height of burr vs hole number for all studied drilled holes

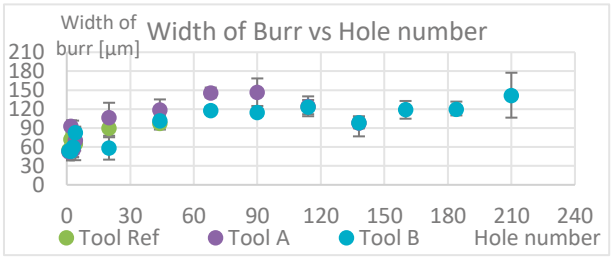

Figure 9: Comparison of the width of burr vs hole number for all studied drilled holes

In Figure 8 and 9, start to compare tool Ref and tool A. Tool A has a high range of height and width of the burr due to higher drilling length, which will create the BUE on the chisel edge during the drilling operation. To compare tool A and tool B, tool B has a small range value of burr information. It can be due to the less BUE on the chisel edge and chippings on the cutting edge by an accumulation of BUE. The chipping starts at hole number 160. Since the criteria of tool life is flank wear reaching 0.2 mm, the drill bits keep drilling.

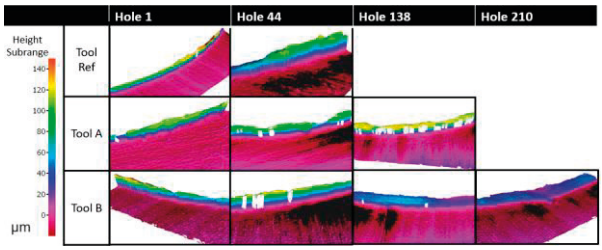

Figure 10: 3D images of burr formation

3.5. SURFACE ROUGHNESS

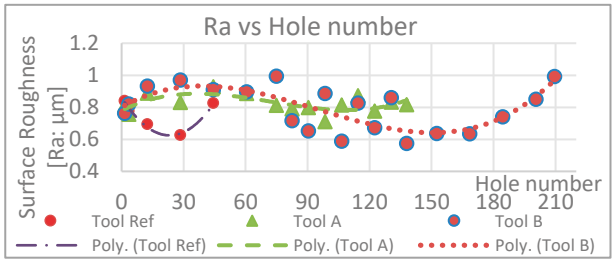

Figure 11: Comparisons of R_a by three drill bits

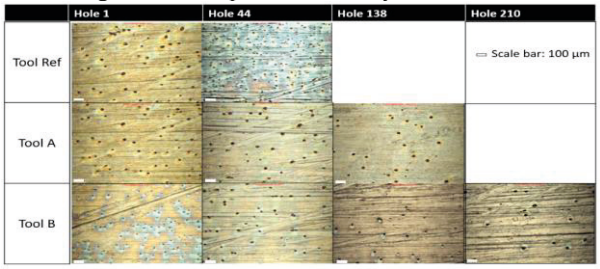

Figure 12: Surface topography of specific holes by three drill bits (10X magnification)

Figure 10 shows 3D images of locally burr formation, which can check the accuracy of results in Figure 8 as a reference. In Figure 11, coated tool A and tool B have the similar tendency of surface roughness variations with hole numbers increases. In Figure 12, the surface topography for specifics holes shows the scratches which explains the unexpected higher surface roughness.

3.6. SUBSURFACE DEFORMATION

Drill bit	Hole number	1	44	138	210
Tool Ref	The thickness of material drag layer (μm)	6.3	7.5		
Tool A		5.6	7.1	9.4	
Tool B		5.7	7.0	9.5	10.0

Table 1:The thickness of material drag layer on specific hole numbers by three drill bits

Microstructural studies of the materials deformations and alterations were conducted using Tescan Mira3 scanning electron microscope equipped with backscatter (BSE) detectors. In Table 1, the thickness is increasing with hole number increases due to the corresponding feed forces. PVD coated tools have lower thickness comparing the same hole number by uncoated tool. When it comes to the end of hole number, the flank wears are similar, but the tool B has higher thickness.

4. CONCLUSIONS

The experimental results show the drills with PVD coating demonstrate substantial increase of the lifetime by improving the wear resistance of drill bits. No obvious difference was observed on surface integrity produced by coated and uncoated drills in terms of roughness and subsurface deformation. However, drills with PVD coatings may causes slightly large size of burr. The drill bit with four cooling channels instead of two has better cooling performance, leads to less flank wear of drill bits and extend the tool life. Moreover, better cooling performance also reduces the diameter variation, size of burr. and has no obvious effects on the surface quality before chippings which are positive to the machined component. Combined with PVD coating and four cooling channels, the tool B has longer tool life, better flank wear resistance and leads to better surface quality before chippings.

ACKNOWLEDGEMENTS

I want to thank Prof. Jinming Zhou, Prof. Rachid M'Saoubi and Dr. Kateryna Slipchenko, as my supervisors at Lund university and industry, to provide the knowledge and give assistances on the experiments when I need help. I want to thank Stefan Frejd at Seco Tools AB for giving me supports on the drilling test, Mikael Hörndahl for sectioning the samples by wire EDM and Dr. Andrii Hrechuk for generous supports.

REFERENCES

[1] T. Yonezawa, *Nickel alloys: Properties and characteristics*, vol. 2. Elsevier Inc., 2012.

[2] J.-E. Ståhl, M. Andersson, and V. Bushlya, *Metal cutting theories and models*. 2012.

[3] A. Hrechuk, V. Bushlya, J.-E. Ståhl, and V. Kryzhanivskyy, "Novel metric 'Implenarity' for characterization shape and defectiveness: the case of CFRP hole quality," *Compos. Struct.*, p. 113722, Feb. 2021, doi: 10.1016/j.compstruct.2021.113722.

[4] Shao Du, "Study on surface integrity in drilling Inconel 718 with uncoated and PVD coated tools," Lund university, 2021.

Machined surfaces as designed cell culture substrates

Kunal Sharma

Department of Mechanical Engineering Sciences
Faculty of Engineering, Lund University
Lund, Sweden

ABSTRACT

Most living cells attach and proliferate on surfaces, but the reasons for attachment are not widely known when it comes to attachment on metal surfaces. Surface roughness is known to have an effect, and some materials are known to be toxic to cells. The aim of this study is to further investigate the effects of surface roughness on cell proliferation through the use of a model adherent cell line. To bridge the current gap in the scope of surface roughness investigations, and establish machined surfaces, i.e. through milling operations, as a valid surface for cell proliferation experiments. Thus, reducing both costs of materials, and the time for sample preparation. The highest cell proliferation was seen at an approximate surface roughness of 0.15 µm. All the samples (AZ31, Al 7075, and Ti6Al4V) except for the Cu-based (CW510L) performed better than the control group after undergoing milling operations. Therefore, establishing these metals and their surface roughness conditions as optimal for future testing and development to ultimately achieve new options to be used as implants in the human body.

1. INTRODUCTION

Certain living cells can attach in a plethora of different ways to surfaces depending on their geometry and surface chemistry. Understanding cell response and proliferation based on material surfaces is vital for various fields of research ranging from clean water supply to human implants [1]. In this area of research, a lot of experiments have been done both *in vitro* and *in vivo* to investigate the physical and chemical properties that affect cell proliferation [2-5]. Very little is known about cell growth and attachment onto machined surfaces. Majority of the researched cell attachment on metals is done through very precise sample preparation in the hopes of achieving specific surface roughness [1]. This study will explore a range of surface roughness values and material types to see how living cells react to the different conditions. One of the main benefits of this study is the juxtaposition of metal samples that are prepared through the traditional method, by grinding, and samples that undergo a milling operation, both yielding good surface conditions for cell proliferation. Combining machining and life sciences in this way allows for a collaboration that can result in quicker and more cost-effective solutions by performing direct experiments on metal surfaces. This study aims at investigating the surface roughness effects on cell proliferation, and determining the optimal surface roughness conditions for the different metals that would be viable options for use as implants in the future.

2. RELEVANT THEORY

There is a good understanding in this field of research that the physical and chemical properties of the material surface affect cell proliferation [2, 4, 6-8]. Huang *et al.* [7] have found that an arithmetical mean surface roughness value (Ra) of 0.15 µm is optimal to achieve the highest proliferation rate. They were able to determine a bell-shaped curve, which can be seen in Figure 1 labelled as areas I and II for cell proliferation within 0.05-1.20 µm range. Keller *et al.* concluded that a rougher surface (sandblasted) experienced an order of magnitude more percent cell attachment when compared to the smooth (1 µm diamond paste polished) surface [6]. This was combined with Huang *et al.*'s conclusion in Figure 1, where III shows Keller *et al.*'s experienced trend.

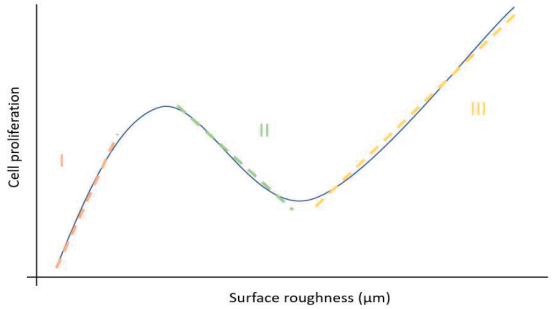

Figure 1: The three experienced surface roughness effects based on the investigated literature currently conducted in the area of cell proliferation

Chung *et al.* concluded that from a nano-scale perspective an increase in surface roughness lead to

better cell attachment which is symbolized as I in Figure 1. On the other hand, [2] has shown opposite findings, where a smoother surface has led to a higher initial adhesion as well as a more increased spreading on the surface. This poses the question, as to whether cell proliferation should only be counted in terms of cell density, or if types of attachment should also be investigated. Therefore, in this study the machined samples will be evaluated based on both cell density, and the type of attachment.

2.1 Metal Specific Properties

Magnesium (Mg) alloys are generally not used as biomaterials due to their poor corrosion properties [9]. However, they have many advantages such as; similar to bone density, they are readily available, have high specific strength even when compared with Ti6Al4V. Li *et al.* investigated the cytotoxicity of magnesium and concluded that there were no inhibitions in cell proliferation with regards to their exposure to magnesium alloys [9].

A lot of research on the chemical properties of metal samples has been conducted in the dental industry. One of the most prominent studies was by Grill *et al.* [5] where they found that Au is effective in maintaining cell viability [4] when combined with other alloying elements as long as the weight percentage (wt.%) is above 71 [10]. Through cell culture tests Craig *et al.* experimented on 29 alloys, and 6 pure metals. The pure metals are of interest to this study and those were: Au, Pd, Ti, Ag, Ni, and Cu. They concluded that Au, Pd, and Ti were least cytotoxic, whereas Cu carried the highest cytotoxicity when compared with the other pure metals [4].

3. Experimental Methods

The metals used are magnesium alloys (AZ61a, AZ31), Cu-based alloys (CW510L), aluminum alloys (Al 7075), and titanium alloys (Ti Grade 2, Ti Grade 11, and Ti6Al4V). All samples went through two processes either grinding for specific surface roughness targeting, or milling with the use of the SECO tool. The samples were imbedded into a resin to allow for easier sample handling. This was done using the Struers CitoPress -5/-15/-30 machine with the MultiFast resin.

Targeting specific surface roughness

The grinding process used in this experimental process was surface grinding using the Struers Tegramin 30 grinding machine. The setup for grinding had to vary based on material hardness, to allow for proper surface roughness targeting. The hardness testing was performed using the Vickers hardness scale. The surface roughness values of Ra and Rt were recorded using the ALICONA IF-MeasureSuite.

Milled surfaces

One sample from each metal group underwent a milling process with the SECO tool (The tool holder: R217.69-2532.0-06-8AN, and tool insert: XOEX060204FR-E03 H15). The cutting data used was the same for all samples: 560RPM, 55 mm/min feed, and 0.05 mm depth of cut. The tool was used with only one insert to allow for a coherent surface finish.

Cell deposition

A549 cells were cultured in flasks until a specific cell density (cells/cm^2) was reached. The cells were lifted from the flask into the F-12K suspension using trypsin which is an enzyme that cleaves focal adhesion points thus removing surface adhesion [11]. PMMA tubes 10mm diameter, 1.5mm thickness, and 10mm height were attached to the areas of interest on the metallic samples using a double-sided tape. The samples, and tubes were all sterilized with 70% ethanol. The cells were then deposited into the tubes. Once deposited the cells were incubated for a period of 48 hours to allow for proliferation. The goals and cell amounts used in the respective trials can be seen in Table 1.

Table 1: Cell quantity and description of experiment for the 3 trials

Experiment	Goal	Number of cells	Goal achieved
1	Determine effects of surface roughness on cell proliferation	17000	Y
2	Determine cell proliferation on machined surfaces	14000	Y

Quantification

Cells were rinsed with phosphate-buffered saline (PBS) solution twice to remove any dead cells from the surface. The cells were fixed during a 15min exposure to 4% paraformaldehyde. The cells underwent an ethanol dehydration series from 30% up to 95% ethanol to allow them to retain their cell morphology in the dried state necessary for secondary electron microscope (SEM) analysis. The surface of the samples was then sputter coated with more than 15nm of Au/Pd. The sputtering was done with chamber pressure 7x10^{-2} mbar, and a current of 15mA, for 250 seconds. This was done due to the non-conductive nature of cells which would result in them charging during SEM analysis, yielding poor image quality. Most of the SEM analysis was performed at 15kV, however for samples where an oxidized layer was present (AZ31, and AZ61a) the accelerating voltage was increased to 20kV. The characteristic sample field view was at 1 or 2mm which allowed for cell counting. The cell counting was performed using image analysis techniques, quantified through area fractions.

RESULTS & DISCUSSION

Ti Grade 2 and Ti Grade 11 were used with varying surface roughness values. Figure 2 shows the images that were taken for 4 different surface roughness values. Through x-ray energy dispersive spectroscopy (XEDS) analysis the cells, which are carbon-based, were determined to be the dark spots in the back-scatter electron (BSE) images.

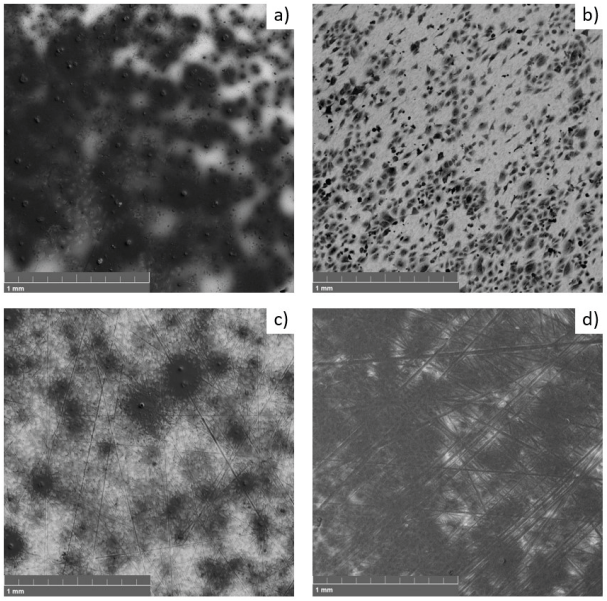

Figure 2: SEM images of the Ti Grade 2 sample using BSE imaging at the various surface roughness specifications; 0.158 µm (a), 0.212 µm (b), 0.263 µm (c), and 0.354 µm (d)

Figure 3 shows that the area fractions for the smoother and rougher surface roughness values are above the threshold. In this case the threshold value is based on the cell proliferation on glass slides which were used as a reference. As previously mentioned by Huang *et al.* the most cell proliferation was seen around a surface roughness of 0.15 µm [7]. Additionally, the rougher end of the spectrum shows an increase in cell proliferation. A further investigation with a larger range of surface roughness values would be beneficial to determine whether 0.15 µm is a local maximum as suggested previously. Chung *et al.* concluded that on a nano-scale an increase in surface roughness leads to more cell proliferation and better cell adhesion [3]. This would suggest that inversely from the 0.15 µm surface roughness the cell proliferation and adhesion should decrease. Or if this increase in cell proliferation continues increasing with reduced surface roughness as suggested by [2]. Since the literature related trends were observed in this method testing experiment, it is valid to assume method correctness.

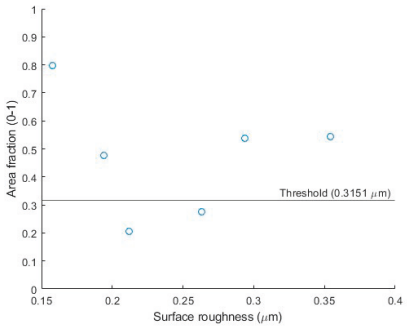

Figure 3: Area fraction graphical representation for the Ti Grade 2 and Ti Grade 11 samples, with the 'Threshold' value from the Glass (reference)

MACHINED SURFACE ANALYSIS

The goal of classifying the cells into specific groups is to identify which samples performed best in terms of cell density, and whether cells attached. The first is easy since it is a direct result of the area fractions which can be seen in Figure 4. To determine whether the cells attached and were thriving in the metal conditions the shape and surrounding areas around the cells were analyzed. Firstly, if the cells were adhered and thriving the areas around the cells would be a lighter shade of grey with carbon deposits which would be the result of the cells spreading and adhering on a larger area. Secondly, the actual shape of the cells can be used to determine if the cells deemed the surface as toxic, or uninhabitable. If the cells were more circular in shape, they were in an environment that is not as prosperous when compared to cells that were of a more elongated/amorphous shape.

Figure 5 (b) shows the CW510L sample which consists of copper-rich environments which are known to be toxic to cells, as a result the cells remained in circular shapes and did not spread out. This is consistent with previous research [4, 5, 10], however a preferred attachment site can be seen. An XEDS spot analysis would be beneficial in order to determine if the less copper-rich surface was the one with higher cell attachment.

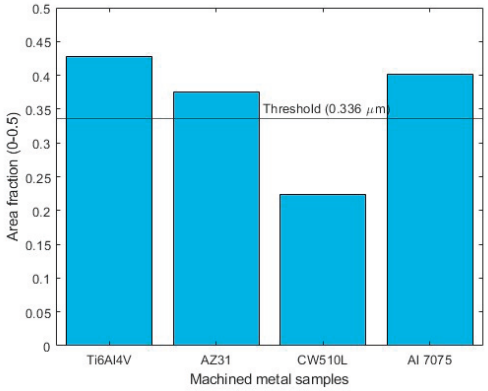

Figure 4: Area fraction values for cell proliferation for the milled samples compared to the threshold value of 0.336 µm

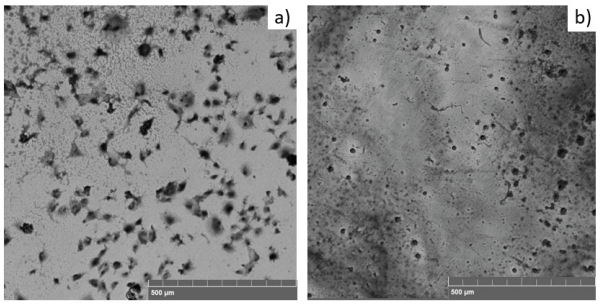

Figure 5: BSE images of different cell attachment types; (a) amorphous cell spreading, (b) circular cell spreading

Figure 5 (a) shows the Ti6Al4V sample and the cells in their amorphous shape Table 2 shows the ranking of the different samples based on their attachment.

Table 2: Cell attachment type

Sample	Cell attachment type
7075 Al	Amorphous
AZ31	Slightly amorphous
CW510L	Circular
Ti6Al4V	Amorphous

CONCLUSION

The highest cell proliferation was seen around 0.15 µm. The two lowest cell proliferation results were seen in the middle range of surface roughness values at 0.212, and 0.263 µm. Both of these results were also below the control sample. All the samples (AZ31, Al 7075, and Ti6Al4V) except for CW510L were above the threshold value of 0.3364 µm. Ti6Al4V and Al 7075 showed clear amorphous shapes meaning the cell thrived on those surfaces. AZ31 was considered 'slightly amorphous' which meant that some of the cells looked circular, while most exhibited an amorphous shape. CW510L was seen to only contain circular shaped cells. Finally, AZ61a did not yield any conclusive results due to a heavily oxidized layer which prevented cell counting. The thesis findings can be used as a suitable workflow for future evaluation of cell proliferation on metal surfaces. It can be further utilized as a screening process for future implants based on the proliferation requirements.

ACKNOWLEDGEMENTS

The author thanks Filip Lenrick and Martin Hjort for their continued support and supervision. Mikael Hörndahl for his guidance in sample preparation. Daniel Johansson from SECO Tools AB for their assistance in tool selection.

REFERENCES

[1] *B. Boyan, "Role of material surfaces in regulating bone and cartilage cell response," Biomaterials, vol. 17, no. 2, pp. 137-146, 1996-01-01 1996, doi: 10.1016/0142-9612(96)85758-9.*

[2] *K. Anselme et al., "The relative influence of the topography and chemistry of TiAl6V4 surfaces on osteoblastic cell behaviour," Biomaterials, vol. 21, no. 15, pp. 1567-1577, 2000-08-01 2000, doi: 10.1016/s0142-9612(00)00042-9.*

[3] *T.-W. Chung, D.-Z. Liu, S.-Y. Wang, and S.-S. Wang, "Enhancement of the growth of human endothelial cells by surface roughness at nanometer scale," Biomaterials, vol. 24, no. 25, pp. 4655-4661, 2003-11-01 2003, doi: 10.1016/s0142-9612(03)00361-2.*

[4] *R. G. Craig and C. T. Hanks, "Cytotoxicity of Experimental Casting Alloys Evaluated by Cell Culture Tests," Journal of Dental Research, vol. 69, no. 8, pp. 1539-1542, 1990-08-01 1990, doi: 10.1177/00220345900690081801.*

[5] *V. Grill et al., "The influence of dental metal alloys on cell proliferation and fibronectin arrangement in human fibroblast cultures," Archives of Oral Biology, vol. 42, no. 9, pp. 641-647, 1997-09-01 1997, doi: 10.1016/s0003-9969(97)00055-1.*

[6] *J. C. Keller, "Tissue Compatibility to Different Surfaces of Dental Implants: In Vitro Studies," Implant Dentistry, vol. 7, no. 4, pp. 331-337, 1998. [Online]. Available: https://journals.lww.com/implantdent/Fulltext/1998/07040/Tissue_Compatibility_to_Different_Surfaces_of.12.aspx.*

[7] *H.-H. Huang, C.-T. Ho, T.-H. Lee, T.-L. Lee, K.-K. Liao, and F.-L. Chen, "Effect of surface roughness of ground titanium on initial cell adhesion," Biomolecular Engineering, vol. 21, no. 3-5, pp. 93-97, 2004-11-01 2004, doi: 10.1016/j.bioeng.2004.05.001.*

[8] *R. Lange, F. Lüthen, U. Beck, J. Rychly, A. Baumann, and B. Nebe, "Cell-extracellular matrix interaction and physico-chemical characteristics of titanium surfaces depend on the roughness of the material," Biomolecular Engineering, vol. 19, no. 2-6, pp. 255-261, 2002-08-01 2002, doi: 10.1016/s1389-0344(02)00047-3.*

[9] *L. Li, J. Gao, and Y. Wang, "Evaluation of cyto-toxicity and corrosion behavior of alkali-heat-treated magnesium in simulated body fluid," Surface and Coatings Technology, vol. 185, no. 1, pp. 92-98, 2004-07-01 2004, doi: 10.1016/j.surfcoat.2004.01.004.*

[10] *D. Brune, "Metal release from dental biomaterials," Biomaterials, vol. 7, no. 3, pp. 163-175, 1986-05-01 1986, doi: 10.1016/0142-9612(86)90097-9.*

[11] *M. A. H.R.H Patel, I.S. Shergill, Basic science techniques in clinical practice, British Library: Springer-Verlag London Limited, 2007.*

[12] *K. Sharma, "Machined surfaces as designed cell culture substrates", Master's thesis, Department of Mechanical Engineering Sciences, Lund University, 2021.*

Measuring Product Dimensions during Assembly

A study in collaboration with Volvo GTO

Hilda Andersson, Serhat Koca

Department of Mechanical Engineering Sciences
Faculty of Engineering, Lund University
Lund, Sweden

ABSTRACT

Volvo Trucks is one of the largest and most successful actors in the automotive industry and delivers trucks all over the world. The company offers trucks that can be customized and adapted according to the customer wishes. Offering highly customizable trucks puts a lot of stresses on the system which requires that CAD-drawings, component documentation and all databases are synchronized and updated according to the changes done on the truck. It has been observed within the company that the actual dimensions of the trucks do not always coincide with the system dimensions. The deviations in dimensions of the truck causes problems during transports as the trucks either exceeds or fall under the system dimensions. The objective, having the above in mind, has been to achieve a better understanding of how different measurement techniques can be used as an automated system for industrial inspection. The aim was to collect data to enable a root-cause analysis on the deviations. Some pre stated factors and causes, and consequences were justified by the measurements and analyzation of data, while others were rejected.

1. INTRODUCTION

A global company within the automotive industry delivers trucks all over the world which makes the planning for transports and logistics a key factor for staying competitive. The truck industry delivers products that are highly customized which means that the trucks fluctuate in dimensions and specifications with a high frequency.

1.1. BACKGROUND

Volvo Trucks uses several different databases for documenting and tracking the trucks, enabling for control and communication within the Volvo Group and external stakeholders. The databases are used in different fields and for different applications. There are databases used by the sales-department and the dealers to provide necessary information such as tender and lead time to customer. Other databases are being used by the production to provide necessary information for the planning and by the logistics for the outbound transports. Even though the databases are being used for different applications they are interconnected and changes regarding the truck information in one database will most likely affect the information in another database used for another application.

Information regarding the truck dimensions is used for planning and estimating the costs of the outbound and order transports. This requires that information regarding the truck, such as the dimensions are correct.

1.2. PROBLEM DESCRIPTION

Volvo offers both variants (standard) and customer adapted trucks (CA), which means that each truck is unique in its dimensions. It has been observed within the company that the actual dimensions of the trucks do not always coincide with the theoretical dimensions.

The deviations in dimensions of the truck causes problems during transports as the trucks either exceeds or fall under the system dimensions. These deviations causes problems such as increased material and immaterial damages, longer transportation lead times, freight costs and impact to the relation with the carriers. There are also aspects around the liability for both Volvo and carrier connected to the dimensions of the load or cargo.

1.3. OBJECTIVE & RESEARCH QUESTIONS

The objective is to achieve a better understanding of how different measurement techniques can improve automated industrial inspection and enable a more solid foundation for root-cause analysis.

The aim is to evaluate and present an optimal vision technique for automated industrial inspection by using literature study and testing analysis. With this scope in mind, the following research questions has been raised:

- What are the economic consequences and how does the current situation affect the relation to the stakeholders, internal- and external customers, transport partners and competitors?

- What kind of measuring techniques exist and how well do they perform in regard to the set requirements?
- What are the root causes of these deviations?
- What aspects should be considered when integrating a future measuring solution to the production process?

2. METHOD

2.1 INTERVIEWS

Interviews were carried out to get a general insight to the company, understand the causes and consequences of the deviations and identify important aspects for the future implementation of an automated system. The interviews were carried out with employees at Volvo, suppliers of measuring equipment, external integrators, competitor for benchmarking and carriers for outbound transports.

2.3 EXPERIMENTAL METHODS & EVALUATION

In the evaluation of different measurement equipment, requirements and criteria in collaboration with the company were defined. The sensors performing the best in the evaluation process were ordered from the supplier to be tested in two different setup conditions, controlled environment and demanding environment.

The controlled environment tests were performed for analyzing the accuracy as a function of different conditions. Two different objects were used during the testing to analyze how well the sensor performed with regards to the object size, shape, contour and color. The demanding environment test was performed to obtain data for the hypothesis testing and to identify the optimal mounting position of the sensors.

The performance in terms of measurement accuracy was evaluated by a statistical model by using hypothesis testing. A null hypothesis was stated for maximum acceptable range of deviation.

3. THEORY

3.1 MACHINE VISION

Modern machine vision systems can be categorized in PC-based vision systems, embedded vision systems and smart cameras, with varying application range, performance and complexity degree as seen in Figure 1. Smart cameras are a complete solution with embedded lenses, sensors, processors, camera-to-computer interface and software, enabling for control and calibration directly on the device itself, lowering the complexity. The compact design of smart cameras and easy functions enables for a wider application range. However, smart cameras are also limited to the memory-size and software interface and its capabilities, lowering the performance level. PC-based systems usually consists of several devices interacting with each other to provide the required vision system. This enables for high customization and performance level, but also requires advanced programming and hardware knowledge. The embedded system as seen in Figure 1 is a hybrid of the smart camera and PC-based system. An embedded microprocessor, enables to be directly connected to an external PC that can be used for programming, controlling and calibration of the sensor.

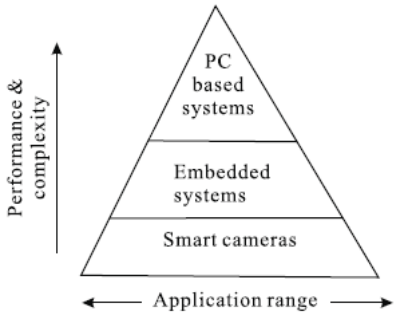

Figure 1 Overview of three machine vision techniques [1].

3.2 LIDAR

LiDAR, an acronym for light detection and ranging is a technology that are well-known and can be used for different measurements equipment. The LiDAR technology can be used for both 2D- and 3D sensors and are being used in a wide range in industrial applications but also in other areas. These sensors make it possible to generate a 3D point cloud of the studied object and the point cloud can be generated in a software. The technology is used widely in the automotive industry for self-driving cars where the demands are high on the techniques, as it requires high resolution, long-range and real time performance and a tolerance to disturbances such as environmental conditions. LiDAR is one of the technologies that can meet these requirements and is therefore used in these kinds of applications.

The LiDAR working principle is based on counting the time between the events when a beam of infrared light is emitted and then the backscattered energy from the pulsed beam is measured. From these time measurements, the speed of light in air is used for computing the distances. This is referred as the time-of-flight (TOF) principle.

5. RESULTS

5.1 RESEARCH QUESTION 1

if the truck is too high, accidents on the road can occur when the truck drives under a bridge that has a maximum height of 4 meters for example. If the dimensions are not correct, there is risk for collision between truck and bridge and the consequences can be very crucial, both in regard to damage of truck but also to humans. Second, if the truck is too high during loading on the vessel, there can also be damage to the trucks. When the carriers are planning their loading process on the vessel, the margins for the height of the vehicles are small, so basically there is no room for deviations. The decks on the vessels are flexible, meaning that it is possible to adjust the height of the deck and the carriers wants to maximize the space on the vessel, which means that it is of high importance that Volvo state correct measurement data. The accidents that can occur in regard to this, is collision between the deck on the vessel and the roof of the truck.

The company are paying freight costs for transport overseas in volume prices. One of the carriers are performing control measurement of the truck in the harbor, right before loading and if there is deviations, the carriers will send new updates of the invoice, which in turn result in a higher freight cost. If the truck is too high, this is obvious but for the case of when the truck is too low, the carriers are assumed to not update the invoice which means Volvo will pay more than needed and also be unaware of this kind of deviation.

Short shipping is the event that occurs when the trucks are left in the port and cannot be loaded on the vessel due to incorrect dimensions, recently the trucks that was short shipped were 4 cm higher than stated. This kind of event is crucial for the company in many aspects. First, Volvo will not be able to deliver the truck to the customer in time as short shipped trucks will have to wait until the next departure. The transport time on the vessels can be long, up to a month and next departure to the destination might be only three or four times per month. Second, the freight costs will increase as they need to book new transports for the trucks. Furthermore, Volvo will have to repair the damaged truck if possible or produce a new truck. Violating regulations can lead to lawsuit and fines, further increasing the costs.

5.2 RESEARCH QUESTION 2

There were three main weaknesses identified for the MRS1000 sensor: the importance of the opening angle, distance to measured object and the difficulties to detect small objects. The results from both the controlled environment and the more demanding one showed that if the opening angle were too wide, the measurement accuracy become worse and were not able to give accurate values relative to the target value. However, if the opening angle was too small, the sensor could not capture the whole width of the truck.

The conclusions that were drawn from the results with the other sensor, O3D302 were similar to the first one. The weaknesses identified for this sensor was the sensitivity to certain colors such as black or white. This sensor really faced difficulties when measuring objects in the mentioned colors, which could be crucial when measuring trucks with these kinds of colors. The strengths identified for this sensor was the ability to detect small objects and the possibility to even provide high accuracy at large angles. Although the sensor showed good performance in measurements of small objects, the drawbacks with the colors was a too important factor that needed to be considered carefully.

5.3 RESEARCH QUESTION 3

Insufficient synchronization is related to the dimensions in company databases and are derived from CAD drawings where all component dimensions are added, providing a total dimension of the truck. Two different causes for insufficient synchronization have been identified. In some cases, the system dimensions are not updated according to customer adaptions (CA), changes that can have a noticeable effect on the dimensions. In other cases, the system dimensions have not been updated for trucks, modified prior to handover to the carriers, modifications that can have noticeable effect on the dimension.

Two different errors affecting the dimensions were identified. The dimensions in the system assumes that the boggy-axle is in its lowest position. A deviation can occur if the boggy-axle is not lowered down during the measuring moment. The dimension in the system assumes that the spoiler is installed in the lowest level. The measuring dimension will deviate from the system deviation if the spoiler has a different installation level at the measuring moment.

From the interviews it was possible to identify different root causes for the factors listed. The root causes are divided into four groups. Equipment and systems describe possible causes related to CAD-engineering and the databases, legislation describes possible causes due to laws and regulations related to transport dimension in Sweden, management describes the possible causes due to the leadership and company culture and transportation describes the number of modifications made on the truck in the activities after production to handover to the carriers.

6. DISCUSSION

6.1 MEASUREMENT RESULTS

Initially in the master thesis, the aim of the work was to implement an automated measurement process in the production plant. With this goal in mind, the objective with the evaluation and selection process of the measurement equipment was to ensure that the equipment could fulfill these requirements. First, implementing an automated process in a production plant will involve several departments and parties in the organization. The production planning needs to be involved as the measurement process needs to be added as a new activity in the production, this includes integrating it as a new activity in the production planning system, but it will also add time to the total production time. The industrial communication plays an important part in the implementation of an automated measuring process as well, therefore skilled engineers in programming and industrial automation is required, preferable if the competence is available internally in the company. Understanding and learning the IT-structure in the company turned out to be a challenging task for us, mostly due to the complex structure of the databases but also for our lack in knowledge and experience regarding databases, programming and data extraction.

6.2 ECONOMICS

When the thesis started it was assumed that the major costs would be due to trucks that were too high. However, it became apparent afterwards that these trucks would only result in extra administrative work for managing the locked invoices and manually updating the system. Trucks that are too high will only require an update according to the correct height, in other words, Volvo will be charged for the correct volume. However, too high trucks also increase the risk for material and immaterial damages during transportation overseas and on land. It also increases the risk for lawsuits and receiving fines. Thankfully, such incidents are scarce, but they would require a different measure of action to investigate and provide documentation for the causing factors which could increase administrative work and other overhead costs.

During the thesis it become more apparent that too low trucks would result in unnecessary payments as Volvo would be charged for a larger volume than required. It was therefore interesting to investigate how many trucks that were too low to be able to estimate the amount of unnecessary costs Volvo was being charged for. Estimating the number of too low trucks was done by investing the Wallhamn report and cross-check that with the Tuve measurements. Prior to investigating the reports, it was expected and assumed that the number of too high trucks and too low trucks would be almost equal, with perhaps some variations. However, the Wallhamn report and Tuve measurements showed that only a small number of trucks had a smaller dimension than the system dimension which went against our assumption.

Considering the administrative work for managing the invoices and manually updating the system, one can link the locked invoices to the Tuve production. It was possible to see a correlation between the number of No-FTP, filtered based on departments, reason and carriers and the number of reported trucks from Wallhamn. Thus, estimating the amount of time spent on receiving and correcting locked invoice could be achieved. The costs due to locked invoices could be divided into costs due to locked invoices and manually updating the system. It was also mentioned that both of these tasks were interlinked and communication between the responsible employees (transport planner and invoice manager) was taking place. Both employees did estimate the amount of time they were spending on receiving the invoices and manually updating the system. However, the invoice manager gave a general estimation for all invoices, but there was a correlation in number of locked invoices and the number of reported trucks from Wallhamn. Their tasks were also interlinked and therefore it could be assumed that the invoice manager is setting aside similar amount of time as the transport planner. Based on this the combined total administrative time for the invoice manager and transport planner due to deviations can be estimated to a few hours every week.

6.3 THE FACTORS AND CAUSES

The process for identifying the causes can be described as having a reverse approach. The process started by determining the factors that led to the deviations and afterwards identifying what root causes were behind the emergence of this factors.

7. CONCLUSION

This thesis provided a great opportunity to investigate the potentiality of an automated measuring system, to see what benefits, and also what disadvantages such a system would bring. The objective of using the system for measuring the trucks during the root-cause analysis was not achieved. Mainly due to the lack of time, but also due to the difficulties faced when calibrating and programming the sensor to achieve reliable and accurate measurements. It should however be mentioned that the struggle of trying to use the sensor for measuring the trucks provided a lot of knowledge and data which we believe would be of great value for Volvo. The root-cause

analysis was still accomplished, using a manual ruler stick which worked better than expected.

Some pre stated factors and causes, and consequences could be justified by the measurements and analyzation of data, while others were rejected.

References

[1] H. U. Zheng Liu, Pradeep Ramuhalli, Kurt Niel, "Integrated Imaging and Vision Techniques for Industrial Inspection," 2015.

Method of Extraction of Lead from Copper alloys

With focus on Brass and Bronze Recycled Materials

Deepak Ram Chandrasekaran, Manish Basavaraj Basaligundi

Department of Mechanical Engineering Sciences
Faculty of Engineering, Lund University Lund, Sweden

ABSTRACT

With recent developments and advancements in technology in the 21st century, the copper industry faces challenges in lowering the lead content of copper alloy scraps due to stricter regulation for lead usage. Lead is a significant concern to the environment under categorised hazardous material. This study accumulates knowledge of all possible lead separation methods and tests one method i.e., Compound separation using Ca-Si to see the validity of claims and further investigates the behaviour of lead and other alloys in slow cooling, quick cooling, and Ca-Si compound separation method at high temperatures. It could be observed from the experiment that around 20% of lead could be removed from the brass and bronze alloys through Ca-Si separation method.

1. INTRODUCTION:

Copper also known as red metal is the third most important metal used by mankind from the days of its existence. Innovation of copper alloys begins from the prehistory period which accounts for mainstream industrialization, but addition of lead is more in the recent years to improve copper alloys machinability. Lead is the heaviest metal found on the earth's crust, customarily mixed with ores of zinc and copper, but it is a significant concern for the environment, and many lead compounds are categorised as hazardous. So, removal of lead is a customary in upcoming years. Experiment of compound separation method was performed and the results were analysed for better understanding of lead behaviour during this process.

2. ALLOYS OF COPPER:

2.1. Brass: Brass is a universally used alloy of copper-containing 65% of copper and 35% of zinc. Leaded brasses are common in industrial usage, with 3-5 % of lead content which enhances machinability and wear resistance. Alpha brasses contain a minimum of 63% of copper to a maximum of 70%. With higher copper content, they tend to be more ductile. Alpha brass is well known for its excellent cold working ability. Duplex brasses are composed of 38-42 % zinc and the rest copper with a small percentage of lead and used in hot working. The small amount of lead added to this brass improves their forging quality, reduces chip breakage, and upgrades the overall machinability of the material [1].

2.2. Bronze: Bronze was one of the early metallic alloys. The alloy of Bronze traditionally extracted from copper and tin, with the evolution being from nearly four thousand years. Modern-day Bronze contains tin, which is substituted by metals such as aluminium, Manganese and even zinc up to some extent. Bronze has some unique properties. Alloying with tin or other metals makes it a lot harder than copper. Bronze is more fusible, which means that it can quickly reach a melting point, making it easier to cast. Commercial Bronze comprises 90% copper, and 10% zinc and architectural Bronze consists of 57% copper, 3% of lead, 40% zinc are more appropriately referred to as brass alloys because zinc is the primary alloying component. Lead in bronze prevents the rusting of the metal as Bronze is primarily used in architectural applications [1].

3. LEAD USAGE AND REGULATIONS:

Lead's value to its pure form in alloy comes with its superior characterisation of low melting point, chemical reactivity, resistance to corrosion and ability to soften at a low melting point. The general policy is usually to limit the emissions to the lowest level in technological terms, and, where possible, recycling would usually be done economically. Lead is registered under REACH with EC/ List no: 231-100 - 4 and CAS no: 7439-92-1 as lead is categorised as hazardous by the European Union with the Harmonised Classification and Labelling's (CLH). The United States Environmental Protection Agency has passed several laws relating to lead. These laws address lead in paint, dust, lead in the environment, lead in water, and lead waste disposal. Under these rules, the EPA is tackling lead poisoning and the associated risks in various areas, including by issuing and imposing regulations. Japan in 2003 passed a regulation on leaching of lead which was limited to 0.01 mg/L. The main intention was to contain the harmful health effects caused by lead exposure. [1].

4. LEAD SEPERATION METHODS:

4.1. *Lead removal by sonochemical synthesis:*

Copper oxide nanoflower is obtained at low temperature at a high yield rate. The details of the synthesis and characterisation of copper oxide (CuO) nanoflowers is analysed. The performance of this material as an adsorbent material for the removal of lead ions (Pb2 +) in aqueous solutions was then evaluated which is a tested lead removal process by Bhanjana et al. The size of the nano flower is around 20 to 90nm at the monoclinic phase. The lead removal in this process with a maximum absorption capacity of 188.7 mg/g at an absorbent close to 0.5mg/mL. The CuO nanoflower method is the best-proposed method for the treatment of wastewater [1].

4.2. *Lead removal from Brass scrap using dilution method:*

The inflow of brass scrap into the EU has been steadily increasing in recent years, despite efforts to reduce the inflow. Hilgendorf et al. conducted 5 to 10 dilution cycles with rod mills where they found the lead content can be reduced to 0.1wt%. With a short-observed return, it was conclusive that lead-free rod production was possible in the future, although the market for lead-free Brass is not as dominant as for leaded Brass [1].

4.3. *Lead separation by Vacuum Distillation method:*

Vacuum distillation of leaded Brass is tried and tested the method using slag from Lead and Zinc from an economic standpoint. Vacuum distillation was carried out at 950- 1100°C and external 1m bar pressure. By liquid condensing metallic Zn condensate of 96wt% was found followed by copper of 99.5wt% in ingot was obtained. Furthermore, with the addition of FeO and SiO2, fayalite-based slag was generated containing lead in order to maintain the material concentration. It was observed that lead evaporates with the reduction of zinc level to less than 0.1wt% [1].

4.4. *Lead separation by Ca-Si Compound:*

This method employs a compound Ca-Si to remove the lead from brass and bronze along with the addition of NaF. The trial was split into two phases in which the Ca-Si compound is first introduced, and the NaF is second. 3kg of Brass (JIS CAC203) has a lead content of 2.15 % mass, and 5kg of bronze (JIS CAC406) contains a lead of 5.5% of the total mass used here in this experiment. They were melted using a 20kw high-frequency induction furnace in a carbon crucible under a nitrogen medium Nakano et al. The first stage involves heating brass to around 1000ºC and introducing and maintaining the $CaSi_2$ Compound to enable the brass to react for 10-15 minutes. The agitated lead particles float to the top surface of the melt, which is skimmed off completely. It was observed by Nakano et al. that after 10 mins of adding the Ca-Si compound, the lead removal remains the same even if held for another 30 minutes, and this implies that the reaction between lead and Ca-Si compound is quick and the aggregated Lead compounds are expected to reach the surface of the melt in 10-15 mins. In the same way for bronze, the Ca-Si compound is added at 1000 ºC when the bronze is in a molten state and held for 10-15 mins. It was observed that nearly 20 % of lead is removed from bronze at the end of the first stage. The amount of Ca-Si compound added to brass was 4% of its total mass, and for bronze, it was 7-8 % of its mass; after this amount, it attains a saturation limit, and the amount of lead removed does not vary upon more addition of $Ca-Si_2$. After skimming the Ca-Si compound at the second stage, the aggregation agent NaF is added at 1050 ºC for brass and 1080ºC for bronze with another holding time of 10-15 minutes. More lead that was not removed earlier by the Ca-Si compound is now expected to be removed. After the last process, the melt is cast and allowed to solidify to study the lead particles presence by XRF and EPMA. Nakano et al. claim that this method proves to remove around 83 % of lead from brass and 82 % of lead from bronze after the second stages in both. Few traces of Ca and Si are expected to be found after the procedure completion, further removed by oxidation refining [1].

5. METHODOLOGY:

The compound separation method using Ca-Si was performed on a lab scale at the Lund university workshop. NaF method was eliminated, considering the high risk involved to perform on a laboratory scale and the non-availability of a nitrogen medium furnace to perform the task. JM5 Johnson metal AB Bronze containing 75-77 % of copper, 4.75-5 % of lead, 8.5 % of tin, 0.2 % of Zinc, and 0.5-0.6 % of nickel was machined, and chips of about 500g are collected, the same way brass chips of 500g containing 55-57% of copper, 3-4.5 % lead and 38-40% zinc were used here. In the furnace, 100 g of brass and bronze were heated to 900-1100 ºC within a ceramic crucible. Trials of both brass and bronze were done to determine the optimal temperature for the task to achieve a flawless melt with minimal zinc removal. Finally, the brass chips were melted for 35 minutes at 1080 ºC. A total of six samples were to be analyzed. One sample of both brass and bronze to be used as a reference material, where they will be melted and quickly cooled at room temperature. Another two samples of brass and the bronze heated to 35 minutes and then allowed to solidify slowly for 24 hours inside the furnace. These samples are then cut along the center and bottom/top parts that has to be of about 1cm and they are packed into epoxy. They are grinded, polished with fine grain size sheets until a scratch free even surface is obtained to be studied in Scanning electron microscope [1].

6.RESULTS:

6.1. Quick cooling of brass

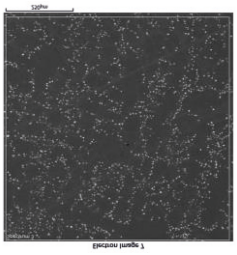

Figure 1. Backscattered image of quick cooling of Brass

In the process of quick cooling, the solidification of lead occurs, which is confirmed by white spots in the Backscattered electron image which is dispersed throughout. The grain size of the lead is about 3-5µm. The specimen has highest wt% of Copper at 61.53%, followed by Zinc at 36.23%, Lead at 2.02% and minimal presence of Iron at 0.22%. Possible reason for the presence of iron could be due to the impurities present in the specimen [1].

6.2. Quick cooling of bronze

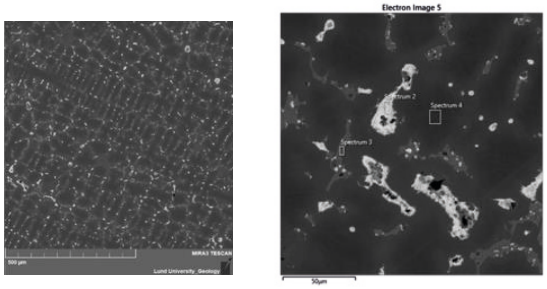

Figure 2.2. a)Secondary imaging of quick cooling Bronze b)Backscattered Image of quick cooling Bronze

We could see the white spots of lead being dispersed widely throughout the matrix in an irregular pattern as seen in the **fig.2a**. Tin and Nickel are also spread evenly throughout the matrix. Lead wt % is found to be 2.26 – 2.41% at different spots of the quick cooled sample. **Fig.2b,** shows the zoomed in closer image at about 150 µm. After quantitative analysis of spectrum 2, it was evident that lead is present in higher wt. percentage of about 92.36 % with some oxygen and copper at 3-4 %. The spectrum 3 contains slight traces of nickel with 72.5 % copper and 24.4 % tin. The spectrum 3 and 4 have no traces of lead [1].

6.3. Slow cooling of bronze

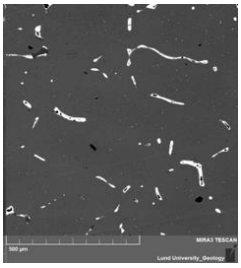

Figure 3. Backscattered image of slow cooling of Bronze

On analysis of this sample, lead is not widely dispersed like the quick cooled bronze, here they are seen as they have clubbed together to form long elongations inside the matrix. The grain size of lead is observed to be slightly bigger than the reference sample 1 but apart from that the lead content does not vary much compared with the quick cooling [1].

6.4 Slow cooling of brass

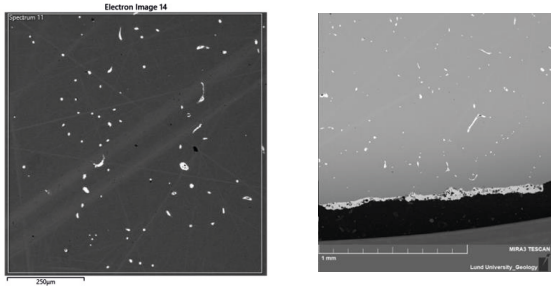

Figure 4. a)Secondary imaging of slow cooling Brass b)Backscattered image of slow cooling of Brass

In theory, a similar trend was expected to be observed in lead separation compared to the reference material. However, after mapping of the image significant reduction of lead is found to be around 0.68wt%. In the process of slow cooling of brass, not much of the lead and zinc separation is observed, but the loss of zinc is 6wt% higher than the reference material. The following figure **fig.4b** represent the SEM imaging of the slow cooling of the brass specimen, closer to the bottom of the crucible. There is a clear separation in the phase observed in the imaging. Due to slow cooling, most of the lead content in the brass specimen has settled to the bottom of the crucible compared to the previous image at various spots. The overall wt.% of copper was found to be higher compared to the reference specimen [1].

6.5. Compound separation of bronze

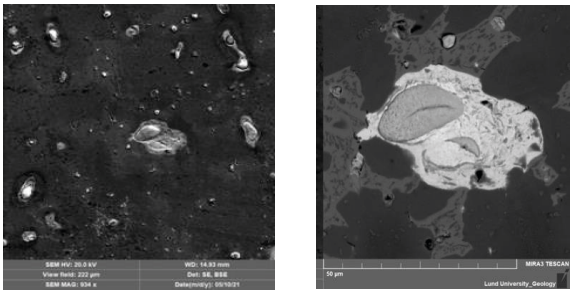

Figure 5.a)Secondary imaging of Ca-Si in Bronze
b)Backscattered image of Ca-Si compound in Bronze

The above image fig.5 shows **Fig.5a** represent the Pb-Ca intermetallic being formed in globules throughout the area analyzed, but they did not float to the top surface of the melt as expected in large, so the lead removal is minimal (approx. 20%) as claimed by the author. This could be due to the fact that the temperature and holding time could have been a bit higher as the reaction between lead and Ca-Si compound is more temperature dependent. Another possibility for the Pb-Ca intermetallic could not make it to the surface would also be presence of O, as this method should be performed under nitrogen medium, which was a limitation for this lab scale experiment. The Lead is surrounded by calcium which could be observed in the above **fig.5b** [1].

6.6. Compound separation of brass

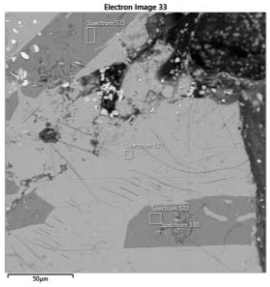

Figure 6. Backscattered image of Ca-Si compound in Brass

The **fig.6** represents the Backscattered imaging of Ca-Si in the brass specimen. Having analyzed various spectrum on the brass sample, the presence of lead was very minimal. The solid-state reaction of the samples could not be achieved despite heating the brass Ca-Si specimen above 1000ºC at different time intervals. Heating the brass chips with Ca-Si above 1000ºC led to the ignition of the sample in the crucible, which may have caused a reaction of zinc from brass leaving behind the solid chips. Copper remains unaffected throughout the reaction [1].

7. DISCUSSION:

Lead behavior was analyzed in slow cooling, quick cooling, and addition of Ca-Si compound to brass and bronze chips at 1100ºC. Initial results from scanning electron microscopy suggested the presence of lead in Bronze was found to be on the higher side ranging to maximum of 92 wt% w.r.t. to slow cooling, quick cooling, and addition of Ca-Si. While the Brass sample resulted in a high presence of Zinc as compared to lead in quick cooling. Whereas in slow cooling, the presence of lead was found to be around 80 wt% at certain spectrums and minimal at few spectrum. On addition of the Ca-Si compound resulted in less than 0.6 wt% presence of lead in brass and less than 2% in bronze.

8. CONCLUSION:

Currently there is no specific working method followed in industries to separate lead from copper alloys. The lead removal from the addition of Ca-Si compound to brass and bronze removes around 20 % of lead, which is not high enough. There is current research on fluorine free compound separation method but those results were found to be only slightly better. So, the future scope would be to try and analyze the lead behavior and removal rate with the addition of NaF to the Ca-Si compound mixture at improved holding time and different temperatures.

ACKNOWLEDGEMENT:

We thank our Supervisors Jakob Johansson and Filip Lenrick for their constant feedback and support to make this project successful. We also thank Lund University (Department of Production and Materials Engineering), who provided us with the opportunity to do the experiments at the workshop and providing with all necessary equipment and materials.

REFERENCE:

[1] - D. Chandrashekaran, M.B.Basaligundi, Methods of Extraction of lead from Copper alloys- with focus on Brass and Bronze recycled materials(2021)pp1-76..

New era of automation in Scania's manufacturing systems

- A method to automate a manual assembly process

Authors: Moutoz Abdalrahman and Alistair Brice

Summary:

Today's car and truck industries are perceived as having complex production systems and relatively high manufacturing expenses, such as labour cost, which is usually combined with complex and unergonomic assembling tasks. A shift towards automation is one solution to eliminate such tasks while increasing productivity and lowering labour costs.

Many products and assembly operations are designed to be performed manually, which creates additional challenges to re-shape these operations so that machines can carry them. The future is here, and what used to be manual, repetitive, and inefficient can now be automated. This master thesis suggests a potential solution of a fully automated assembly line of a steering wheel and front wheel on a pedal car; developed, tested, evaluated, and finally implemented in Scania's Smart Factory Lab.

The study can be seen as a potential base and a physical demonstrator for implementing such a system in an actual assembly line and has proven that even manually designed tasks can be automated without a need for redesigning the process or the components involved. The study includes designing, testing, and implementation of some of the main automation system components, including the physical resources within the production line for the pedal car. This is followed by a summary of the challenges faced regarding the automation system components. Finally, a method to transform manual assembly operations into automated is suggested. The method is flexible and applicable for any manual assembly process if the technology required is available.

Keywords: Industry 4.0, Automation, Robot, Production.

Tribological Performance of Ferritic Nitrocarburizing (FNC) Treated Automotive Brake Discs

CHANDAN KUMAR RAVINDRA REDDY, SHANMUKHARAJ JAYASANKAR

Division of Production and Material Engineering
Faculty of Engineering, Lund University
Lund, Sweden

Abstract

A braking system is used to decelerate or stop the vehicles. The automobile manufacturers search for the better advancement of the brake discs materials to improve quality, reduce wear, corrosion, and more service life. However, due to stringent government regulations in particle emission from automobile brake wear, the poor corrosion resistance of Gray Cast Iron (GCI) brake disc materials has become a significant source of concern for automakers in recent years and coming years. So, the innovative solution to overcome the problem is Ferritic NitroCarburizing (FNC) is treated on the GCI. This study aims to investigate the tribological behavior of the FNC treated automotive GCI brake discs and untreated GCI brake discs. The three different brake discs that are used in experimentation i) Gray Cast Iron (GCI), ii) Ferritic NitroCarburized (FNC) treated GCI, and iii) Post oxidized FNC treated GCI brake discs (Corr-i-durr). The tribo-testing machine is used to analyze the tribological behavior of the different brake discs, which is the coefficient of friction and wear. The brake pads used in all these experiments are of Non-Asbestos Origin (NAO) material. The samples are prepared and etched to analyze the microstructures using the Scanning Electron Microscope (SEM) and Alicona Microscope. The Microhardness of the brake discs is measured using the Vickers Hardness indentor. The results from the tribo-testing machine where the Coefficient Of Friction (COF) and wear depends on the sliding velocity and pressure applied and how it changes when these values are varied are plotted. FNC treated GCI material shows high COF and wear compared to the other materials.

Keywords: GCI, FNC, COF, Wear, Tribology

1. INTRODUCTION

In recent years, the automobile industry has experienced rapid growth. In every aspect, the automobile industries are working to make the betterment of their product. In that braking system is one. Brake systems are a common feature of aircraft, cars, cranes, wind turbines, and other mechanical machinery. The brake disc and brake pads are essential components in the system that are mainly used to decelerate or stop moving vehicles.

Electric Vehicles (EVs) and hybrid vehicles are another factor that will boost the global automotive brake market. The regenerative braking principle is used in EVs braking system. In regenerative braking, the kinetic energy produced by the wheel is converted to electrical energy, and it is stored in the motor during braking, deceleration, or downhill running. Regenerative braking is always not enough when there is a need for emergency braking to stop the vehicle, so there is a combination with friction braking to get enough braking power to stop the vehicle. Since the friction brakes are used less or occasionally in the EVs, and the brake disc rotors are made of the GCI, there will be corrosion problems in the electric vehicle.

GCI brake discs have poor corrosion resistance and wear performance; they are a great concern to the automotive industries. It is believed that brake failure due to the corrosion of the brake disc will be rampant in the future when electric vehicles have dominated the transportation market thoroughly. The automotive industry is currently seeking better and cheaper approaches to controlling these problems.

This project aims to determine Ferritic Nitrocarburized treated brake discs tribological behavior which is considered to show high wear resistance and corrosion resistance compared to GCI. This is to understand how the FNC treated GCI brake disc results when the tribotest is performed compared to the untreated GCI brake disc. The vehicle braking performance is dependent on the tribological properties of the brake disc and brake pads. The aim is to understand the alternative solution is theoretically capable of being implemented as a transportation solution. So that we can replace it with the GCI brake disc in the EVs in upcoming years.

2. METHOLODOGY

A small piece is cut from the brake disc where the cross-section should contain the coated layer for the sample preparation. The sample is etched to enhance the better microstructure characteristics. The microstructure is analyzed using Alicona and Scanning Electron Microscope (SEM).

For the tribological behavior measurements, the tribotester machine is used. The test matrix is created using different velocities and contact pressure, which we can see in the below table.

Table 1: Test Matrix

Test Condition	P_1=0.75 Mpa	P_2=1.5 Mpa	P_3=2.5 Mpa
V_1=0.1m/s	100 passes	100 passes	100 passes
V_2=0.3m/s	100 passes	100 passes	100 passes

For every workpiece material, 6 conditions are performed, which are mentioned in the test matrix. Each tool perform the conditions like Tool 1 for GCI for velocity 0.1m/s and pressures 0.75MPa, 1.5MPa, 2.5 MPa. So the COF and wear rate are determined from the experiments.

The surface roughness and hardness is also calculated by using the profilometer and the Vickers hardness intender.

3. RESULTS

3.1 MICROSTRUCTURE

The FNC samples have the same microstructure shown in the Figure 1. FNC samples have the compound layer which is formed by the diffusion of carbon and nitrogen into the surface. The compound layer thickness of the nitrocarburized samples was examined in etched condition. The post oxidised FNC will have an oxidized layer over the compound layer. But the additional oxidized layer is not found in the Corr-I-Durr sample. These FNC samples have the compound layer of range 10µm to 50µm. The thickness of the compound is not uniform. The uniform thickness may be due to the increase in the carbon content of the substrate. Pores are visible in the outer part of the compound layer in the Ferritic nitrocarburized and the post-oxidized FNC sample.

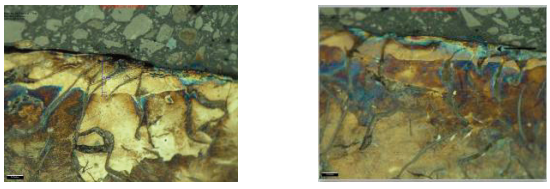

Figure 1: compound layer and pores present in the microstructure of FNC material.

3.2 SURFACE HARDNESS

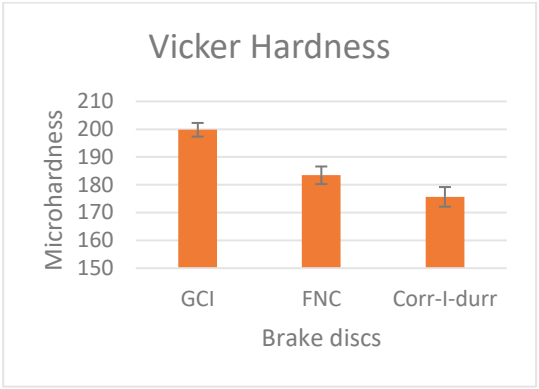

Figure 2: Vickers hardness

In Figure 2, it can be seen that the GCI brake discs have high higher hardness when compared to the FNC and Corr-I-Durr brake discs. This is because the compound layer of the Ferritic nitrocarburized samples is not homogenous through the surface, and the hardness of the FNC depends on the depth of the compound layer. Corr-I-Durr shows lower hardness comparatively to FNC-treated GCI and the untreated GCI. The composition of the base material also determines the hardness of the surface. If the carbon content is low, it forms the softcore over the surface, resulting in the lower hardness for the FNC brake discs. In the nitrocarburized samples, the micro indentor breaks the compound layer and reaches the surface, resulting in lower hardness compared to untreated GCI.

3.3 SURFACE ROUGHNESS

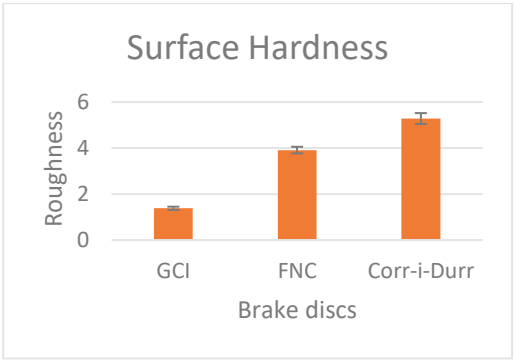

Figure 3: surface roughness of brake discs

From Figure 3, it can be observed that Corr-I-Durr brake discs have higher surface roughness compared to the untreated GCI. This roughness is measured before the experiment. The roughness of the brake discs depends on the material constituents present and machining.

3.4 Coefficient Of Friction

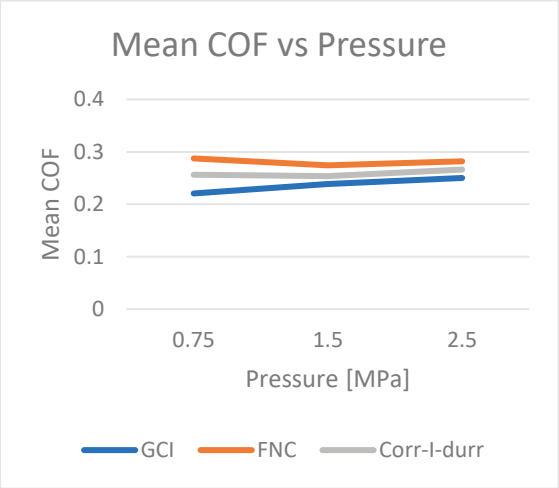

Figure 4: Mean Coefficient of friction vs different brake discs with varying pressure for velocity 0.1m/s

Figure 4 shows that Mean COF decreases with increasing pressure for the certain velocity 0.1m/s. The COF is high initially and gradually decreases for the pressure 1.5MPa. For 2.5MPa the COF start to increase. And the FNC treated brake discs shows high COF.

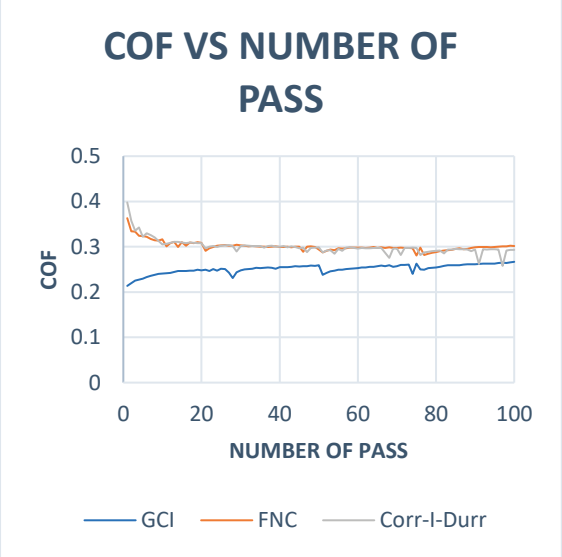

Figure 5: COF for 100 passes

3.5 Wear

Figure 5 shows that wear coefficient decreases with increases with pressure for constant velocity. Corr-I-Durr material shows a high wear coefficient.

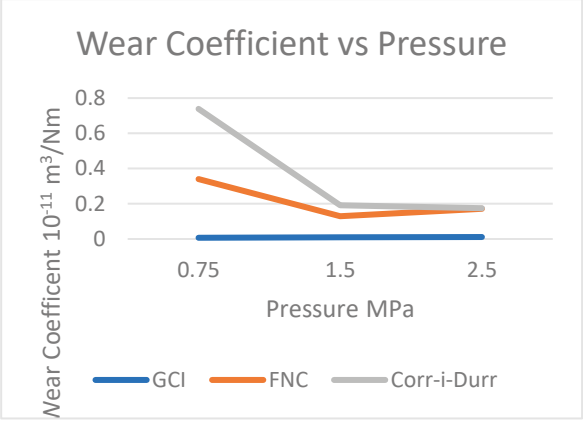

Figure 6:Wear Coefficient for velocity 0.3m/s with varying pressure

4. Discussion

The coefficient of friction is considered to be the important parameters that qualify the braking performance and safety. The coefficient of friction depends on the operating conditions such as sliding velocity, pressure, temperature, etc. For the constant velocity and increasing the braking pressures, the coefficient of friction starts to increase initially, and then the COF begins to decrease. This effect of braking pressure is mainly through their contact area. When the braking pressure increases, the actual area of contact will increase, increasing COF But when the increment ratio of the contact area is smaller than the applied pressure, the coefficient of friction starts to fall.

This can be observed from the above Figure 5, for the FNC treated brake discs, the COF starts to decrease for the increasing pressure that means the actual area of contact between the pads and discs must have reached the steady value, and this contact area ratio should be lower than the applied pressure.

As the tribological theory, when the sliding velocity is low, the frictional heat produced between the brake pads and discs will be low. So the increase in sliding velocity will increase the surface temperature between the sliding pairs, which leads to the formation of the tribofilm. The tribofim are produced with a certain thickness, with an increase in temperature. Once the tribofilm is formed, the cof gradually decreases and attains a stable value. The tribofilm consists of carbon consists of carbonaceous reaction products, unreacted constituents, oxide from the metallic ingredients. The Ferritic Nitrocarburized treated brake discs also show a decrease in the COF This also attributed to the formation of the tribolfilm,

consisting of abrasive particles from the pad materials. As the temperature increases the tribofilm starts to shear, and then COF tends to increase.

Figure 4 shows that the mean coefficient of the three different brake discs starts to decrease. This is because the newly produced brake discs will have the spiral ridge pattern resulting from the turning operation, and this will gradually wear off.

The friction depends on the microstructure of the brake discs. The amount of graphite present in the GCI will influence an increased coefficient of friction. The friction also depends on the surface irregularities between the discs and pads. As the FNC treated, brake discs have higher surface roughnesss compared to the untreated GCI. So the FNC treated brake discs show a higher coefficient of friction.

The brake pads slide against the brake discs during the tests, causing wear loss in both discs and pad material. The brake pads used for the Ferritic Nitrocarburized brake discs show a high weight loss compared to the untreated Gray cast iron. The GCI observed lower weight loss despite the higher hardness.

The wear behavior increased with the load; this may be due to the quick plastic deformation of the material in the contact surface. After that, the real contact area will increase, making an anti-wear effect. As the mechanical actions between the asperities become more with the velocity increases, the wear rate rises with the velocity.

It can be seen from Figure 6; initially the wear loss is high for the FNC brake discs. Then when the braking pressure increases, the wear loss starts to decrease, with the formation of tribofilm. The thickness of the tribolayer affects both the coefficient of friction and wear loss. When the braking pressure is further increased and the tribolayer is destroyed producing the high particles on counterface, increasing the wear loss.

Theoretical literature says that compound layers contain ε phase, which implies excellent wear resistance. But in this experiment, the FNC treated brake discs have significantly shown a high wear rate than the untreated GCI.

The surface roughness also plays a major role in the wear rate. As the FNC treated brake discs show higher surface roughness, the weight loss of the brake pads for the FNC discs is high. The brake pads are slide continuously against the discs for a long time, and different conditions cause the wear.

5. CONCLUSION

The thesis aims to understand how the FNC surface treated GCI brake discs perform in their tribological properties and compare them with the untreated GCI. The results from the tribological experiments and the microstructure of these samples were analysed and concluded.

- The braking pressure and the sliding velocity have a higher effect in the friction coefficient and wear.
- The tribofilm formed during the experiment over the surface acts as a protective layer.
- The FNC brake discs have a higher coefficient of friction, about 0.27 compared to the GCI, about 0.24.
- The thickness of the nitrocarburized compound layer will determine the efficiency of the brake discs, and the compound layer is not uniform throughout the surface.
- As the brake pads show a high amount of weight loss when used for FNC brake discs, it will affect the braking performance. So it is suggested that Gray cast iron will be the better material for brake discs.

ACKNOWLEDGMENTS

We would like to express our sincere gratitude and thanks towards our supervisors

- Jens Wahlström– Lund University,
- Samuel Awe – Automotive Components Floby AB
- Oleksandr Gutnichenko- Lund University
- Rebecca Lindvall- Lund University

REFERENCES

C. K. RAVINDRA REDDY and S. JAYASHANKAR, "Tribological Performance of Ferritic Nitrocarburizing (FNC) Treated Automotive Brake Discs," Lund University, Lund, 2021.

Wear Investigation of Metal Matrix Composite (MMC)

Hema Kalidasu, Manideep Beri

Department of Production and Materials Engineering
Faculty of Engineering, Lund University
Lund, Sweden

ABSTRACT

The thesis subject is dedicated to use Tungsten Carbide (WC) as reinforcement for Hadfield steel. WC is mainly considered for its combination of high hardness and good toughness. The microstructure characteristic of WC was analyzed using an Optical microscope (Alicona), Scanning Electron Microscope (SEM), Hardness Vickers Test, and Wear lab tester. The compositions used for this work have shown good mechanical results. The interface between Hadfield steel and the reinforced region has shown a strong metallurgical bonding. Finally, MMC have shown good wear resistance properties.

1. INTRODUCTION

The main aim of the current thesis is to develop a Metal Matrix Composite (MMC) reinforce with WC particles. Currently, industries have shifted their focus on the development of materials with overall properties such as MMC materials. These latter demonstrated highly attractive properties.

2. METHODOLOGY

This thesis has started with a proper introduction mentioning the background. A detailed study was carried out to gain immense knowledge on MMC, Hadfield steel, WC, and manufacturing methods. The Materials used, their specification, and compositions are derived from previous experiments. The materials were prepared following powder processing technology. The prepared MMC samples were studied using different characterization techniques. Microstructure analysis was carried out using Optical Electron Microscope (Aliconaa), Scanning Electron Microscope (SEM), and mechanical characterization was performed using Vickers Hardness tester. Finally, a wear test was performed on the final composite samples.

3. EQUIPMENTS USED

The project involves different characterization equipment. The list of equipment used and their applications are described below

Name of Equipment	**Application**
Lathe	Mixing of raw materials
SEM-EDS	Chemical Analysis
Pressing Machine	Compacting raw materials
Struers Cutting Machine	Sample Preparation
Struers Hot Mounting Machine	Sample Preparation
Struers Tegramin 30	Sample Preparation
WEDM	Cutting Samples
OEM (Alicona)	Microstructure Characterization
SEM	Microstructure Characterization
Vickers Hardness Tester	Mechanical Characterization
Lab Wear Test	Wear Resistance Characterization

TABLE 1: LIST OF EQUIPMENT USED

4. RESULTS AND DISCUSSION

A total of 21 samples were selected to be studied. Due to the limited access to equipment and COVID restriction, only 8 samples could be analyzed. The samples B*05, C*XB1, B*0, and C*1 are selected for the wear test based upon their mechanical results. We could see that the WC particles have been homogeneously distributed; no cracks or pores were found. There is a clear and defect-free interface layer between the matrix and reinforcement in all the samples. The hardness has increased compared to the base alloy. The wear test has shown promising results. The wear ratio has decreased in all MMCs compared to the matrix.

5 CONCLUSION

In summary, Tungsten Carbide (WC) particles were successfully reinforced with Hadfield steel. Study of morphology, mechanical properties, and wear analysis on WC reinforcement investigated through Optical

microscope (Alicona), SEM, hardness measurement and followed by wear Test.

The conclusions are:

- WC particles reinforced Hadfield steel have shown good microstructural analysis. No defects such as pores and cracks have been found.
- All MMC samples have shown a strong metallurgical bond between the matrix and the reinforced region.
- A gradual increase in hardness has been found in the composite zone compared to the matrix (base alloy).
- A notable improvement in the wear performance of MMC has been achieved compared to the matrix.

6. Abbreviations and Acronyms

WC- Tungsten Carbide

MMC- Metal Matrix Composite

OEM- Optical Electron Microscope

SEM- Scanning Electron Microscope

EDS- Electron Dispersive X-Ray Spectroscopy

WEDM- Wire Electrical Discharge Machining

Acknowledgments

We want to thank our company and LTH supervisor, Dr. Latifa Melk, for her constant support and guidance throughout the thesis.

We want to express our gratitude to all the staff at the IPROD workshop for their assistance and Sandvik R&D test site manager: Michael Hybelius, for his help during the wear testing.

References

[1] Wear Performance Investigation of Metal Matrix Composite (MMC) by Hema Kalidasu and Manideep Beri

Printed by Media-Tryck, Lund 2021 NORDIC SWAN ECOLABEL 3041 0903

This book includes the summaries of the
Master's degree works conducted by the students in
the Production and Materials Engineering program,
Lund University during the spring 2021.
The full length versions can be found on
the Lund University homepage.

MSc Program

Production and
Materials
Engineering

Mechanical Engineering Science

2021

LUND UNIVERSITY

LTH
FACULTY OF
ENGINEERING

Production and Materials Engineering
Department of Mechanical Engineering Sciences